FU JEN CATHOLIC UNIVERSITY

50 YEARS OF SERVICE

To The People

of

CHINA

1929 — 1979

FU JEN STUDIES

NATURAL SCIENCES

NO. 13 1979

CONTENTS

FU JEN UNIVERSITY

TAIPEI, TAIWAN, REPUBLIC OF CHINA

NOTE ON ORIENTABLE RULED SURFACES IN E^3 — CONTINUED

YI-CHING YEN

1. PRELIMINARIES

In a previous paper[1], I found some properties of the conoid by studying the total mean curvature of orientable ruled surfaces in E^3. In this note, I shall give some other characterizations of conoids. By a conoid I mean a ruled surface which passes through a curve with its generators parallel to a plane. We shall discuss the following:

Theorem 1. Let an orientable noncylindrical ruled surface M have a vector form

$$\vec{x}(u, v) = \sigma(u) + v\,\delta(u)\,, \tag{1}$$

where $\sigma(u)$ is a base curve and $\delta(u)$ the director curve of M, $\|\delta\| = 1$. Then M is a conoid if and only if

$$r = (\delta'', \delta', \delta) = 0\,. \tag{2}$$

Theorem 2. Let M be a conoid with vector form $\vec{x}(u, v)$ as in (1), where $\sigma(u)$ is the striction curve and $\delta(u)$ the unit-speed director curve of M. Then

1) M is a right conoid if and only if

$$\sigma' \cdot \delta = 0 \tag{3}$$

2) M is a helicoid if and only if

$$\sigma' \cdot \delta = 0 \quad \text{and} \quad p(u) = \text{constant}\,, \tag{4}$$

where p is the distribution parameter of M.

Theorem 3. Let a right conoid M in E^3 have a vector form as (1), where $\sigma(u)$ is the line of striction and $\delta(u)$ the unit-speed director curve of M. Then the asymptotic curves of M other than u = constant have the expression for v as

$$v = C\sqrt{|p(u)|} \tag{5}$$

where p is the distribution parameter and C is an arbitrary constant. Equation (5) also expresses the distances from the line of striction to the asymptotic curves.

Corollary. On a helicoid M in E^3, the helices form a system of parallel curves and are geodesic parallels of M.

2. THE PROOFS

Proof of Theorem 1. For brevity, let the director curve δ in (1) be unit-speed, so that $\|\delta'\| = 1$. The vectors $\delta(u)$ drawn from the center 0 of the unit sphere $\Sigma : x^2 + y^2 + z^2 = 1$ form a curve C on Σ, and δ'' is the curvature vector of C, hence $\delta'' \neq 0$. Since $\delta \cdot \delta' = \delta' \cdot \delta'' = 0$, if in addition

$$r = (\delta'', \delta', \delta) = 0,$$

then the 3 non-zero vectors δ'', δ' and δ are coplanar together with $\delta' \perp \delta$, $\delta'' \perp \delta'$ imply that

$$\delta'' = k\delta. \tag{6}$$

Then all the osculating planes of C spanned by δ' and δ'' pass through 0, and it is known[2] that C becomes a plane curve on Σ, i.e. C is a circle with the expression of curvature vector as (6), then C is a great circle of Σ, δ'' being directed toward 0, we have $k = -1$, i.e.

$$\delta'' = -\delta. \tag{7}$$

If C takes the position vector

$$\delta(u) = (\cos u, \sin u, 0), \tag{8}$$

then the ruled surface M with the expression (1) has its generators passing through the base curve σ and parallel to the xy-plane. Hence, by definition, M is a conoid.

Conversely, if M is a conoid, we express it as (1) with director curve δ given in (6). Then it is easily shown that $(\delta'', \delta', \delta) = 0$.

If δ in (1) is not unit-speed, we may reparameterize it as

$\delta(u) = \mu(s)$, where $s = h(u)$ is the arc length of μ, and let $\sigma(u) = \sigma(h^{-1}(s)) = \lambda(s)$. Then the vector function $\vec{x}(u, v)$ now becomes

$$\vec{x}(h^{-1}(s), v) = \vec{Y}(s, v) = \lambda(s) + v\,\mu(s)\,. \tag{9}$$

Thus, by (4), M is a conoid if and only if $(\mu''(s), \mu'(s), \mu(s)) = 0$. Since $\delta'(u) = \mu'(s)(ds/du)$ and $\delta''(u) = \mu''(s)(ds/du)^2 + \mu'(s)(d^2s/du^2)$, we have

$$(\delta''(u), \delta'(u), \delta(u)) = (\mu''(s), \mu'(s), \mu(s)) \left(\frac{ds}{du}\right)^3 = 0. \quad \text{q. e. d.}$$

From now on, without loss of generality, we take the base curve σ as striction curve and u the arc length of the director curve δ. Then we have for an orientable noncylindrical ruled surface M the expression (1) with the conditions

$$\sigma' \cdot \delta' = 0\,, \tag{10}$$

$$\|\delta\| = \|\delta'\| = 1\,. \tag{11}$$

If for a conoid M, its director curve δ takes the form in (6), then applying the equation of (10), we have the striction curve σ as

$$\sigma(u) = \left(\int g(u)\cos u du,\ \int g(u)\sin u du,\ h(u)\right) \tag{12}$$

for every continuous function g and differentiable function h. Hence, by (1), the conoid M has the vector representation

$$\vec{x}(u, v) = \left(\int g(u)\cos u du + v\cos u,\right.$$
$$\left.\int g(u)\sin u du + v\sin u,\ h(u)\right) \tag{13}$$

Equation (13) may be regarded as the general form of a conoid.

Proof of Theorem 2. If

$$a(u) = \sigma'(u) \cdot \delta(u) \tag{14}$$

is equal to zero, then together with (10), we have $\sigma' // \delta' \times \delta$. Since $\delta' \times \delta$ is the unit normal vector to the plane to which the generators are parallel, $\delta' \times \delta$ is a constant unit vector α. Let $\sigma'(u) = \phi'(u)\,\alpha$, say, then $\sigma(u) = \phi(u)\,\alpha$. Thus, M has its generators always orthogonal to the line of striction. Therefore, by definition, M is a right

conoid. The converse is a straight forward computation from (13) to get $a(u) = 0$. We can easily obtain the general form of a right conoid from (13) if we apply (8) and (12) to $a(u) = 0$, to have $g(u) = 0$.

If $a(u) = 0$, and the distribution parameter

$$p(u) = (\sigma'(u), \delta'(u), \delta(u)) \tag{15}$$

is a constant k, then we have $\sigma'(u) = k\alpha = \beta$, a constant vector, which implies that $\sigma(u) = \beta u$.

Then M is swept by a moving straight line attached on the line of striction in such a way that it rises and rotates in a constant ratio. Hence, by definition, M is a helicoid. The converse is trivial if we give an explicit vector representation for the helicoid.

Proof of Theorem 3. By [1], we have the DE. of the asymptotic curves of the conoid as

$$du\,[(p'(u)\,v - a(u)\,p(u))\,du - 2p(u)\,dv] = 0\,, \tag{16}$$

M being a right conoid, we have $a(u) = 0$, hence by (16) we have two asymptotic curves $u =$ constant and (5). Since v in (1) is the directed distance along $u =$ constant, say u_0, from the line of striction to the curve $x(u_0, v)$, the distances from the line of striction to the asymptotic curves with the expression (5) have the distances as in (5).

Now we prove the Corollary. Since M is a helicoid, we have $p(u) = k$, a constant. Then equation (5) can be written as

$$v = C\sqrt{|k|} = \bar{C}\,, \tag{17}$$

$\bar{C}$: an arbitrary constant. Thus the asymptotic curves other than $u =$ constant are $v =$ constant, each of (17) is equidistant from the line of striction which has a constant vector β. Also $u =$ constant and $v =$ constant are orthogonal, since $F = a(u) = 0$. The curves, $v =$ constant make a constant angle with the line of striction:

$$\frac{\vec{x}_u \cdot \alpha}{\|\vec{x}_u\|} = \frac{(\sigma' + v\,\delta') \cdot \sigma'}{\sqrt{\sigma' \cdot \sigma' + v^2}\,\|\sigma'\|} = \frac{\beta \cdot \beta}{\sqrt{\beta \cdot \beta + v^2}\,\|\beta\|} = \text{constant}.$$

Hence v = constant are helices, and form the geodesic parallels with the generators u = constant on M.

REFERENCES

(1) Yen Y.C., Note on Orientable Ruled Surfaces in E^3. *Fu Jen Studies*, No. 12, 1978.

(2) Struik D. J., *Lectures on Classical Differential Geometry*, 2nd ed., Reading, Mass., Addison-Wesley, pp. 21, 1961.

"We are not independent entities, alien to Earth. Earth in turn is not adrift in a vacuum unrelated to the cosmos. The cosmos is no longer cold and hostile because it is our universe. It brought us forth, and it maintains our being. We are, in the very literal sense of the words, children of the universe."

ERIC J. CHAISSON

REGULARIZATION OF SINGULARITIES FOR ONE-DIMENSIONAL NONLINEAR HYPERBOLIC SYSTEMS*

NEI-MAO CHEN

ABSTRACT

It is well-known that the Cauchy problem for a linear hyperbolic system will have smooth solutions if the initial data are smooth[1]. Unfortunately, it is not true, in general, that the solutions of a nonlinear system will be smooth even if we have smooth initial data. In particular, if the system is genuinely nonlinear, F. John has shown in his paper[2] that we can not even expect the solutions to be C^2. In this paper we shall study those singularities more closely. And we find that if we choose a new coordinate system the solution will be regularized.

DEFINITIONS

The differential equation we considered here is a nonlinear hyperbolic system

$$u_t + a(u)\, u_x = 0 \tag{1}$$

where $u = u(x, t)$ is a vector with n components $u_1, \ldots, u_n$ depending on two scalar independent variables x and t, and $a(u)$ is an $n \times n$ square matrix. We also assume that the initial function

$$u(x, 0) = f(x) \tag{2}$$

is infinitely differentiable and is of compact support. The local existence of this solution was shown in the book[1].

We assume that the system (1) is strictly hyperbolic, that is, there are n real and distinct eigenvalues $\lambda_1, \ldots, \lambda_n$ of the matrix $a(u)$ for all $|u| \leq \delta$. Let

$$\lambda_n < \lambda_{n-1} < \ldots < \lambda_1 . \tag{3}$$

We denote $\xi^1, \ldots, \xi^n$ the corresponding right eigenvectors (column

* This research is partially supported by the Chinese National Science Foundation and the Research Foundation Fu Jen Catholic University.

vectors) of the matrix a, and $\eta^1, \ldots, \eta^n$ the left eigenvectors (row vectors), respectively. We normalize them in such a way that

$$\eta^i a = \lambda_i \eta^i, \qquad a\xi^k = \lambda_k \xi^k \tag{4}$$

and

$$\xi^k \cdot \xi^k = 1, \qquad \eta^i \xi^k = \delta_{ik}, \tag{5}$$

$i, k = 1, 2, \ldots, n$. We also assume that in the region of consideration the matrix $a(u)$ is smooth in u.

The system is said to be "genuinely nonlinear"[3] in the sense that in the u-space the derivatives of each λ_i in the direction of its corresponding eigenvector ξ^i do not vanish.

NON-EXISTENCE THEOREM IN THE (x, t) PLANE

It is well-known for $n = 1$ or $n = 2$ that the first derivative u_x will tend to infinity at a finite time provided that the system (1) is genuinely nonlinear[4]. When the number of dependent variables is higher than two it is still true that u_x will tend to infinity at a finite time but the proof of this[2] becomes much more complicated.

For $n \geq 3$, we introduce the scalars

$$\omega_i = \omega_i(x, t) = \eta^i \cdot u_x, \qquad i = 1, 2, \ldots, n \tag{6}$$

then we have

$$u_x = \sum_{i=1}^{n} \omega_i \xi^i. \tag{7}$$

Define

$$c_{ikm} = c_{ikm}(u) = \left(\frac{d}{ds} (\eta^i(u)\, a(u + s\xi^m(u))\, \xi^k(u)) \right)_{s=0}. \tag{8}$$

Then genuine nonlinearity implies that $c_{iii} \neq 0$ for all $i = 1, 2, \ldots, n$.

The family of i-th characteristic curves for the system (1) is the solution of the ordinary differential equation

$$\frac{dx}{dt} = \lambda_i(u(x, t)), \tag{9}$$

which we call C_i. Let

$$\frac{d}{dt} = \frac{\partial}{\partial t} + \lambda_i \frac{\partial}{\partial x}$$

denote the directional derivatives along C_i. Then differentiating ω_i along each C_i gives

$$\frac{d\omega_i}{dt} = \sum_{k,m} \nu_{ikm}\, \omega_k\, \omega_m \tag{10}$$

where

$$\nu_{ikm} = \nu_{imk} \tag{11a}$$

$$\nu_{iii} = -c_{iii} \tag{11b}$$

$$2\nu_{iim} = -c_{iim} - c_{imi} + \sum_{j \neq i} \frac{\lambda_j - \lambda_m}{\lambda_j - \lambda_i} c_{ijm}(\eta^j \cdot \eta^i), \quad \text{for } m \neq i \tag{11c}$$

$$2\nu_{ikm} = -\frac{\lambda_k - \lambda_m}{\lambda_k - \lambda_i} c_{ikk} - \frac{\lambda_m - \lambda_k}{\lambda_m - \lambda_i} c_{ikm}, \quad \text{for } k \neq i,\ m \neq i. \tag{11d}$$

Equations (11b) and (11d) yield important relations that

$$\nu_{iii} \neq 0 \quad \text{for all } i$$

$$\nu_{ikk} = 0 \quad \text{for } k \neq i.$$

Note, at $u = 0$, $a(0)$ has eigenvalues $\lambda_1(0), \ldots, \lambda_n(0)$ with

$$\lambda_n(0) < \ldots < \lambda_1(0).$$

We also can choose suitable signs for $\eta^i(0)$ to make $\nu_{iii}(0) > 0$. Then, by the smoothness of these quantities in u, we will have that

$$\nu_{iii}(u) > 0, \quad i = 1, 2, \ldots, n \tag{12}$$

$$\lambda_i(u) < \lambda_k(v) \quad \text{for } k < i, \tag{13}$$

for $|u| < \delta$, $|v| < \delta$ with δ sufficently small.

Let supp $f \subset [\alpha_0, \beta_0]$ with $s_0 = \beta_0 - \alpha_0$. Defining

$$\theta = \sup_x s_0^2 |f''(x)| \tag{14}$$

we have the following

Theorem.[2] There is a positive number θ_0 (depending only on the matrix a and positive number δ) such that, for initial f with $0 < \theta < \theta_0$, the solution $u(x, t)$ of (1) and (2) can not be of class C^2 for all positive t.

The failure of $u(x,t)$ to be of class C^2 for all $t > 0$ arises because one of ω_i defined in (6) becomes unbounded at some finite time. If we introduce

$$W_0 = \sup_{i,x} |\omega_i(x, 0)|, \qquad W_0^+ = \sup_{i,x} \omega_i(x, 0)$$

where $\omega_i(x, 0) = \eta^i(f(x)) \cdot f'(x)$, then one of ω_i will tend to infinity before the time

$$T = \max_i \frac{4}{\nu_{iii}(0)\, W_0^+}. \tag{16}$$

Inequalities (13) imply that, for all $|u| \leq \delta$, there is a real number λ such that

$$\min_{i<k} (\lambda_k - \lambda_i) = \lambda > 0. \tag{17}$$

Let us denote the solutions of (9) by $x = X_i(\sigma, t)$, i.e., $X_i(\sigma, t)$ satisfies

$$\frac{\partial}{\partial t} X_i(\sigma, t) = \lambda_i(u(X_i(\sigma, t), t)), \quad X_i(\sigma, 0) = \sigma. \tag{18}$$

Set $\alpha_i(t) = X_i(\alpha_0, t)$, $\beta_i(t) = X_i(\beta_0, t)$, with

$$t_0 = \frac{1}{\lambda} s_0 \tag{19}$$

we have that, as long as the solution u exists,

$$\beta_i(t) < \alpha_k(t) \quad \text{for } k > i \text{ and } t > t_0. \tag{20}$$

In other words, if we define the region

$$R_i = \{(x, t) \mid \alpha_i(t) \leq x \leq \beta_i(t)\} \tag{21}$$

which is called the i-th characteristic strip, (20) says that $R_i \cap R_k = \phi$ for $i \neq k$ and $t > t_0$.

EQUATIONS IN THE (σ, t) PLANE

Let ω_1 denote the first ω_i tending to infinity, and let $(\bar{x}, \bar{t})$ be the first singular point. John shows that $(\bar{x}, \bar{t})$ is in R_1, and near $(\bar{x}, \bar{t})$ all other ω_i, $i \neq I$ are bounded like $O(\theta)$. We consider the I-th characteristics C_I which is prescribed by the parametrized equation

$$x = X(\sigma, t) \tag{22}$$

i.e., it satisfies

$$\frac{\partial X}{\partial t} = \lambda_I(u(X(\sigma, t), t)), \quad X(\sigma, 0) = \sigma . \tag{23}$$

Define the quantity

$$\frac{\partial X}{\partial \sigma} \equiv \zeta(\sigma, t) . \tag{24}$$

$\zeta = 0$ gives the envelope of the family of curves (22) in the x, t-plane. The second equation of (23) gives

$$\zeta(\sigma, 0) = 1 . \tag{25}$$

Differentiating ζ with respect to t, we obtain

$$\frac{\partial \zeta}{\partial t} = \sum_m c_{Im}\, \omega_m\, \zeta . \tag{26}$$

(For detail, see John[2].) Now we change the independent variables x, t to σ, t by (22) and introduce new dependent variables by

$$\begin{aligned} &v_i(\sigma, t) = \omega_i(X(\sigma, t), t) \\ \text{for} \quad &i \neq I . \\ &v_I(\sigma, t) = \zeta(\sigma, t)\, \omega_I(X(\sigma, t), t) \end{aligned} \tag{27}$$

Next, we look for differential equations for these new dependent variables in the σ, t-plane. Note that in the σ, t-plane the images of C_I are vertical lines. So after suitable calculations we have

$$\frac{\partial}{\partial t} v_I = \sum_{m \neq I} (c_{Im} + 2\nu_{Im})\, v_I\, v_m + \zeta \sum_{k,m \neq I} \nu_{Ikm}\, v_k\, v_m \tag{28}$$

$$\frac{d}{d\sigma} v_i = \frac{1}{\lambda_i - \lambda_I} \left(\sum_{m \neq I} 2\nu_{iIm}\, v_I\, v_m + \zeta \sum_{k,m \neq I} \nu_{ikm}\, v_k\, v_m \right) \tag{29}$$

for $i \neq \mathrm{I}$. (From now on i indicates an index different from I.) Here $d/d\sigma$ means to differentiate along the corresponding characteristics

$$\frac{d}{d\sigma} = \frac{\partial}{\partial \sigma} + \frac{\zeta}{\lambda_i - \lambda_{\mathrm{I}}} \frac{\partial}{\partial t} \tag{30}$$

respectively. To insure that the system (28), (29) is quasilinear, we shall also find differential equations for ζ and u, which give

$$\frac{\partial \zeta}{\partial t} = c_{\mathrm{III}} v_{\mathrm{I}} + \zeta \sum_{m \neq \mathrm{I}} c_{\mathrm{I}m} v_m \tag{31}$$

$$\frac{\partial u}{\partial t} = \sum_{m \neq \mathrm{I}} (\lambda_{\mathrm{I}} - \lambda_m) v_m \xi^m . \tag{32}$$

Therefore, the problem of solving (1) and (2) becomes that of solving the quasi-linear system (28), (29), (31) and (32) with initial conditions

$$\begin{aligned} &v_{\mathrm{I}}(\sigma, 0) = \eta^{\mathrm{I}}(f(\sigma)) f'(\sigma), \quad v_i(\sigma, 0) = \eta^i(f(\sigma)) f'(\sigma) \\ &\zeta(\sigma, 0) = 1, \qquad\qquad u(\sigma, 0) = f(\sigma) . \end{aligned} \tag{33}$$

We note that the strip R_{I} is transformed into the vertical strip $\alpha_0 \leq \sigma \leq \beta_0$ which we may again call R_{I} in the σ, t-plane. We also expect that the image of R_i in the σ, t-plane will at least be far apart from R_{I} after $t > t_0$.

MAIN THEOREM IN THE (σ, t) PLANE

With initial condition $v_i(\sigma, 0) = \eta^i(f(\sigma)) f'(\sigma)$, we set

$$\mathrm{W}_i = \max_{\sigma} |v_i(\sigma, 0)| , \quad \mathrm{W}_i' = \max_{\sigma} \left| \frac{\partial v_i(\sigma, 0)}{\partial \sigma} \right| .$$

We assume that

$$\mathrm{W}_i \leq p\theta, \quad \mathrm{W}_i' \leq p\theta \quad \text{and} \quad \mathrm{TW}_i \leq p\theta , \tag{34}$$

where p is a suitable constant, and T is given by (16). We recall that "constant" means depending only on the matrix a and the positive number δ. Let $(\bar{\sigma}, \bar{t})$ be the image of the point $(\bar{x}, \bar{t})$. We have the

Theorem. The system (28), (29), (31) and (32) with initial condition (33) which satisfy (34) can have a smooth solution in the σ, t-plane in some region containing the point $(\bar{\sigma}, \bar{t})$, provided that θ is sufficiently small. In particular, there exists a smooth solution of u in that region.

Proof. (i) First we change equations (28), (29), (31), (32) together with (33) into integral equations

$$v_I(\sigma, t) = v_I(\sigma, 0) + \int_0^t \Big[\sum_{m \neq I} (c_{IIm} + 2\nu_{IIm}) v_I v_m + \zeta \sum_{k,m \neq I} \nu_{Ikm} v_k v_m \Big] dt \tag{35}$$

$$v_i(\sigma, t) = v_i(\rho_i, 0) + \int_{\rho_i}^{\sigma} \frac{1}{\lambda_i - \lambda_I} \Big[\sum_{m \neq I} 2\nu_{iIm} v_I v_m + \zeta \sum_{k,m \neq I} \nu_{ikm} v_k v_m \Big] d\sigma \tag{36}$$

where the integrations for each $i \neq I$ are taken on (see (30))

$$\frac{dt}{d\sigma} = \frac{\zeta}{\lambda_i - \lambda_I} \quad \text{with} \quad \sigma = \rho_i \quad \text{as} \quad t = 0.$$

$$\zeta(\sigma, t) = 1 + \int_0^t (c_{III} v_I + \zeta \sum_{m \neq I} c_{IIm} v_m) dt \tag{37}$$

$$u(\sigma, t) = f(\sigma) + \int_0^t \sum_{m \neq I} (\lambda_I - \lambda_m) v_m \xi^m dt. \tag{38}$$

Note, in (38), u is a vector function with $u = (u_1, \ldots, u_n)$. We are going to solve (35), (36), (37) and (38) by iterations.

Since all c_{jkm}, ν_{jkm}, λ_j are smooth in u, there is a constant M such that

$$\max_{|u| \leq \delta} \left\{ |c_{jkm}(u)|, |\nu_{jkm}(u)|, \left| \frac{\partial c_{jkm}(u)}{\partial u} \right|, \left| \frac{\partial \nu_{jkm}(u)}{\partial u} \right|, |\lambda_j(u)|, \left| \frac{\partial \lambda_j(u)}{\partial u} \right| \right\} \leq M.$$

Let ψ denote the vector $(v_1, \ldots, v_n, \zeta, u_1, \ldots, u_n)$. We pick $\psi^0 \in C^1$ which is defined on the region bounded by $0 \leq t \leq T + 1$ and two extreme characteristic curves C_m^0, C_M^0 passing through the points $(\alpha_0, T + 1)$ and $(\beta_0, T + 1)$ respectively (see Fig. 1). Such a region

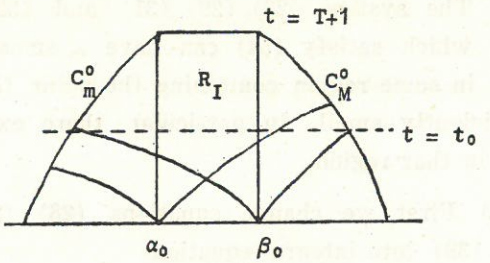

Fig. 1. Characteristic strips in the (σ, t) plane.

we call region G^0. We also require that $\psi^0(\sigma, 0)$ satisfies the initial conditions (33) and its components satisfy

$$|v_i| \leq K\theta, \quad |v_I| \leq K\theta, \quad |u| \leq \delta, \quad |\zeta| \leq M_2 \tag{39a}$$

$$TV \leq K\theta \quad \text{where}$$
$$V = \max\left(\sup_{(\sigma,t)} \sup_{i \neq I} |v_i(\sigma, t)|, \sup_{(\sigma,t)\in R_I} |v_I(\sigma, t)|\right) \tag{39b}$$

$$TV_I \leq M_1 \quad \text{where} \quad V_I = \sup_{\substack{\sigma \in I \\ 0 \leq t \leq T+1}} \{|v_I(\sigma, t)|\}$$

$$T\left|\frac{\partial \zeta}{\partial t}\right| \leq M_3, \quad T\left|\frac{\partial u}{\partial t}\right| \leq M_4\theta \tag{39c}$$

$$\left|\frac{\partial v_i}{\partial t}\right| \leq K\theta, \quad \left|\frac{\partial v_I}{\partial t}\right| \leq K\theta, \quad \left|\frac{\partial u}{\partial t}\right| \leq K'\theta, \quad \left|\frac{\partial \zeta}{\partial t}\right| \leq K'\theta. \tag{39d}$$

Here all constants K, K', M_1, M_2, M_3, M_4 are suitably large and depend only on the matrix a and the positive number δ and n.

(ii) We define ψ^j inductively as follows: Given ψ^{j-1} defined on G^{j-1}, which is bounded by $0 \leq t \leq T + 1/j$ and the curves C_m^{j-1}, C_M^{j-1}, such that $\psi^{j-1} \in C^1$, $\psi^{j-1}(\sigma, 0)$ satisfy (33) and the camponents of ψ^{j-1} satisfy (39), ψ^j is defined on the smaller region G^j which is defined in the same may as G^{j-1}. We define ψ^j componentwise by substituting ψ^{j-1} into the right hand side of equations (35), (37) and (38) which give

$$v_I^j = v_I(\sigma, 0) + \int_0^t \Big[\sum_{m \neq I} (c_{IIm} + 2\nu_{IIm})\, v_I^{j-1} v_m^{j-1} + \zeta^{j-1} \sum_{k,m \neq I} \nu_{Ikm}\, v_k^{j-1} v_m^{j-1} \Big] dt. \tag{40}$$

$$\zeta^j = 1 + \int_0^t \left(c_{111}\, v_1^{j-1} + \zeta^{j-1} \sum_{m \neq 1} c_{11m}\, v_m^{j-1} \right) dt\,. \tag{41}$$

$$u^j = f(\sigma) + \int_0^t \sum_{m \neq 1} (\lambda_1 - \lambda_m)\, v_m^{j-1}\, \xi^m\, dt\,. \tag{42}$$

Since the above integrations are taken along the vertical lines $\sigma \equiv$ constant, the values of v_1^j, ζ^j, u^j are well-defined over the region G^j. We also note that such ψ^0 defined above exists for we may pick $v_1^0(\sigma, t) = v_1(\sigma, 0)$, $v_i^0(\sigma, t) = v_i(\sigma, 0)$, $\zeta^0(\sigma, t) = 1$ and $u^0(\sigma, t) = f(\sigma)$. Before solving for v_i^j, $i \neq 1$, let us point out some lemmas.

Lemma 1. a) $\zeta^j > \frac{1}{2}$ for $(\sigma, t) \notin R_1$, and

b) $\frac{3}{2} > \zeta^j > \frac{1}{2}$ for $t \leq t_0 = (2/3\lambda)\, s_0$ for θ sufficiently small.

The conditions a) and b) in Lemma 1 hold for all ζ^j in the sequence whenever ψ^{j-1} is given except possibly for ζ^0 which will not effect our proof. For convenience, we assume that ζ^0 satisfies a) and b). Lemma 1 says that, after we suitably adjust for those v_i's, the curves $\zeta^j = 0$ lie only in the region R_1 and $t > t_0$.

Lemma 2. All i-th characteristics C_i in the σ, t-plane starting initially at a point on I_0 lie outside of the region R_1 after $t > t_0$ if θ sufficiently small.

We define v_i^j by

$$v_i^j = v_i(\rho_i, 0) + \int_{\rho_i}^{\sigma} \frac{1}{\lambda_i - \lambda_1} \left\{ \sum_{m \neq 1} 2\, \nu_{i1m}\, v_1^{j-1}\, v_m^{j-1} + \zeta^{j-1} \sum_{k,m \neq 1} \nu_{ikm}\, v_k^{j-1}\, v_m^{j-1} \right\} d\sigma\,. \tag{43}$$

the integrations are taken along the correspondent i-th characteristics

$$\frac{dt}{d\sigma} = \frac{\zeta^{j-1}}{\lambda_i(u^{j-1}) - \lambda_1(u^{j-1})}\,. \tag{44}$$

If $\zeta^{j-1} \neq 0$ in the whole region G^j, then (43) gives the values of v_i^j in the whole region of G^j. We now consider the case that curve $\zeta^{j-1} = 0$ lies in the region G^j. $\zeta^{j-1} = 0$ must be in R_1 and $t > t_0$. Denote the intersection of the curve $\zeta^{j-1} = 0$ and the line

$t = T + 1/(j+1)$ on the left by α^j and on the right by β^j. We only consider the case for $\lambda_i > \lambda_I$, that is, $i < I$. Let $\bar{C}_i^j$ be the i-th characteristic which passes through the point (α^j, T^j), where $T^j = T + 1/(j+1)$. The curve $\bar{C}_i^j$ separates the region G^j into two parts; one is the shaded region $\bar{G}_i(\psi^{j-1})$, or simply denoted by $\bar{G}_i^j$, the other one, the unshaded region G_i^j (see Fig. 2). Formula (43) defines the values of v_i^j over the region G_i^j. But for any point in $\bar{G}_i^j$, the curve C_i of (44) may run out of the region G^{j-1} as σ decrease. Formula (43) may not be used to calculate the values for v_i^j in $\bar{G}_i^j$. Nevertheless, since ψ^{j-1} is given in the region G^{j-1}, for points in the neighborhood of $\bar{C}_i^j$, v_i^j can still be calculated from (43). Therefore, we can extend the values of v_i^j into the region $\bar{G}_i^j$ such that $v_i^j \in C^1$ in G^j. If v_i^j satisfy the inequalities (39) in G_i^j, then we can arrange the extension of v_i^j so that they satisfy the inequalities (39) in the whole region G^j. This kind of extension is not unique.

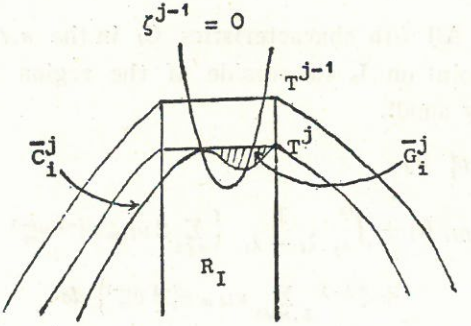

Fig. 2. The Region of G_i^j and $\bar{G}_i^j$.

(iii) The right hand side of (43) contains ρ_i and the relation involving ρ_i and σ, t is given by (44). Let us denote this solution of (44) to be

$$t = \tau_i^j(\sigma, \rho_i) \qquad \text{with} \quad t = 0 \quad \text{as} \quad \sigma = \rho_i .$$

It is always possible to solve ρ_i as a function of σ and t. Moreover, we have the

Lemma 3. $\partial\tau_i^j/\partial\rho_i$ is bounded away from zero uniformly in G_i^j for those ψ^j defined in this iterative scheme. In other words, there is a constant A such that

$$\left|\frac{\partial\tau_i^j}{\partial\rho_i}\right| \geq A .$$

Lemma 3 says that the family of curves given by (45) will not form an envelope.

It is obvious that $\psi^j \in C^1$ and satisfies the initial condition (33). By straight estimate, we can also show that ψ^j as defined above also satisfies inequalities (39). (For details, see Chen[5]). For the contractiveness of the sequence ψ^j, let us consider the ψ^j defined only in the strip $0 < t < h$ and $(\sigma, t) \in G^0$ which we call D_0. Set

$$z^j = \psi^{j+1} - \psi^j$$

with $z = (z_1, \ldots, z_n, z_\zeta, z_{u_1}, \ldots, z_{u_n})$. Componentwise, we can show that there are bounded operators K_1, K_i with $\|K_1\| = O(\theta)$, $\|K_i\| = O(\theta)$ where $\|\cdot\|$ denotes the max norm, such that

$$\frac{\partial}{\partial t} z_1^j = K_1 z^{j-1}$$

$$\frac{\partial}{\partial\sigma} z_i^j + \frac{\zeta^{j-1}}{\lambda_i(u^{j-1}) - \lambda_1(u^{j-1})} \frac{\partial}{\partial t} z_i^j = K_i z^{j-1} .$$

There exist bounded operators K_ζ, $\bar{K}_\zeta$, K_u, $\bar{K}_u$ with $\|K_\zeta\| = \|K_u\| = O(\theta)$ and $\|\bar{K}_\zeta\| = \|\bar{K}_u\| = O(1)$ such that

$$\frac{\partial z_\zeta^j}{\partial t} = (K_\zeta + \bar{K}_\zeta) z^{j-1}$$

and

$$\frac{\partial z_u^j}{\partial t} = (K_u + \bar{K}_u) z^{j-1} .$$

We integrate above from $t = 0$ to $t = h$ and have

$$\begin{aligned}
|z_1^j| &\leq h\|K_1\| \, \|z^{j-1}\| \\
|z_i^j| &\leq (4Mh + s_0) \|K_i\| \, \|z^{j-1}\| \\
|z_\zeta^j| &\leq h\|K_\zeta\| \, \|z^{j-1}\| + h\|\bar{K}_\zeta\| \, \|z^{j-1}\| \\
|z_u^j| &\leq h\|K_u\| \, \|z^{j-1}\| + h\|\bar{K}_u\| \, \|z^{j-1}\| .
\end{aligned} \tag{45}$$

We choose h so small and θ so small that

$$h \max (\|\bar{K}_\zeta\|, \|\bar{K}_u\|) \leq \frac{1}{4}$$

$$\max (h\|K_t\|, (4Mh + s_0)\|K_i\|, h\|K_\theta\|, h\|K_u\|) \leq \frac{1}{4}.$$

Then (45) becomes

$$\|z^j\| \leq \frac{1}{2}\|z^{j-1}\|.$$

Therefore, the scheme is contractive in the strip D_0. Note that this h depends only on δ, n and the matrix a and hence the same procedure can be applied on the strip one step up and so on[5].

(iv) If we start the scheme in the strip $0 < t < h$ with $\psi^0 \in C^\infty$, then we can have the limit function $\psi \in C^\infty$, too. In order to have a C^∞ extension into a region which covers the point $(\bar{\sigma}, \bar{t})$, we pick the next strip to be $h - \varepsilon < t < 2h - \varepsilon$ for $\varepsilon \ll h$. The new sequence ψ^j defined in $h - \varepsilon < t < 2h - \varepsilon$ will converge again to a C^∞ function, which we still call ψ.

In each step, we calculate the value

$$\tilde{t} = \underline{\lim}\, \{t_\zeta \mid \zeta = \zeta^j,\ \zeta^j \text{ is the component of } \psi^j,\ j = 1, 2, \ldots\}$$

where $t_\zeta = \inf \{t \mid \zeta(\sigma, t) = 0\}$. We repeat the above procedure until there is some integer P such that $(P-1)h - (P-2)\varepsilon < \tilde{t} < Ph - (P-1)\varepsilon$. Thus we will have a smooth solution ψ up to $t = Ph - (P-1)\varepsilon$. Note above arguments can not apply to the next strip $Ph - P\varepsilon < t < (P+1)h - P\varepsilon$ since at the new initial line $t = P(h - \varepsilon)$ the tangent of C_i will be parallel to the x-axis.

We make the following conclusions:

(1) For $t < t_P = P(h - \varepsilon) + \varepsilon$, the sequence ζ^j converges to ζ and the lower limit turns out to be a limit, i.e., $\tilde{t} = \bar{t}$.

(2) The point $(\bar{\sigma}, \bar{t})$ is in the strip $t_P - h < t < t_P$. We can pick the final h sufficiently small so that in the final strip, the values of ζ are small and that the strip is under the curves $\bar{C}_i^j$, for $i = 1, 2, \ldots, n$ and for $j \geq N$ for some N. Therefore, the limit function ψ satisfies the differential equations (28), (29)), (31) and (32).

(3) The solution is unique up to $t = \bar{t}$.

(4) The extension over $t > \bar{t}$, particularly for points near $(\bar{\sigma}, \bar{t})$, can not be expected to be unique.

Corollary. The coordinate transfomation (22) is smooth.

Proof. Since $\zeta = X_\sigma(\sigma, t)$ is smooth so is $X(\sigma, t)$.

The coordinate transformation for (x, t) to (σ, t) is smooth. The singularity of the smooth transformation (22) is the curve $\zeta = 0$, and the point $(\bar{\sigma}, \bar{t})$ is a cusp singularity.

REFERENCES

(1) Courant R. and D. Hilbert, *Methods of Mathematical Physics*, vol. II, New York, Interscience, 1961.

(2) John, F., Formation of Singularities in One-Dimensional Nonlinear Wave Propagation, *Comm. Pure App. Math.*, vol. 17, 1974, pp. 377-405.

(3) Lax, P. D., Hyperbolic Systems of Conservation Laws, II, *Comm. Pure App. Math.*, vol. 10, 1957, pp. 227-241.

(4) Lax, P. D., Hyperbolic Systems of Conservation Laws and Mathematical Theory of Shock Waves, *Regional Conference Series in Applied Math.*, SIAM 1973.

(5) Chen, N. M., Analysis of the Singularities for One-Dimensional Nonlinear Hyperbolic Systems, *Ph. D. dissertation*, Courant Institute of Mathematical Sciences, New York University, 1978.

"Praise I. B. M., that boils
the brains rich stores
down to a few
electric either/ors."

JOHN UPDIKE
Midpoint

TWO-PARTICLE CORRELATIONS AND THE STATISTICAL MODEL

JEN-I CHEN

ABSTRACT

Two-particle correlations of high energy multiparticle reactions are calculated and analyzed with a simple statistics model proposed by the author. Comparison with experiments is well discussed.

I. INTRODUCTION

In a previous paper, the author has proposed a simple statistical model[1] for high energy multiparticle reactions, which has interpreted the following phenomena successfully:

1. constant total cross sections;
2. small transverse momenta, but large in wide-angle scatterings;
3. low multiplicity of particles produced;
4. angular distribution of produced particles;
5. single particle inclusive spectrum.

The area of two-particle correlations was left untouched, for the reason that experimental data were not so conclusive at that time. This paper is devoted to investigating this problem for the completeness of the statistical model.

The statistical model is based on the following assumptions:

1. The probability for the reaction from an initial state $|i\rangle$ to a final state $|f\rangle$ is given by

$$|\langle i \mid f\rangle|^2 = \text{const. } I_i \cdot F_f \qquad (1)$$

where I_i is the interaction factor assumed to be

$$I_i = \int dx\, dy\, dz\, dt$$

integrating over the overlapping space-time of the two interacting particles in the initial state. F_f is a decay distribution of the resulting thermodynamics equilibrium state (called fireball), which is assumed to be equally probable for all channels available.

2. The decay volume of the fireball approaches a constant in the high energy limit.

3. All possible particle and resonance states are approximated by an average mass spectrum,

$$\rho(m) = cm^{-5/2} e^{bm} + \sum_i g_i \delta(m - m_i) \qquad (2)$$

where $b = (160\,\mathrm{Mev})^{-1}$, and the second term takes account of low lying discrete states with degeneracy g_i.

Some definitions of relevant quantities should be introduced before proceeding. For the single particle inclusive process,

$$a + b \to c + \mathrm{X}$$

and the two-particle inclusive process,

$$a + b \to c + d + \mathrm{X}$$

where X stands for anything else, the respective normalized single particle and two-particle inclusive spectra are defined as

$$\rho^c_{ab}(\vec{p}_c, s) = \frac{\mathrm{E}_c\, d^3\sigma(a + b \to c + \mathrm{X})}{\sigma_{ab}\, d^3 p_c} \qquad (3)$$

and

$$\rho^{cd}_{ab}(\vec{p}_c, \vec{p}_d, s) = \frac{\mathrm{E}_c\, \mathrm{E}_d\, d^6\sigma(a + b \to c + d + \mathrm{X})}{\sigma_{ab}\, d^3 p_c\, d^3 p_d} \qquad (4)$$

where σ_{ab} is the total cross section. One two-particle correlation function is defined as

$$C^{cd}_{ab}(\vec{p}_c, \vec{p}_d, s) = \rho^{cd}_{ab}(\vec{p}_c, \vec{p}_d, s) - \rho^c_{ab}(\vec{p}_c, s)\, \rho^d_{ab}(\vec{p}_d, s). \qquad (5)$$

For simplifying data collection and presentation in multiparticle reactions, in practice, new variables (called rapidity) y_i are introduced as

$$p_{i//} = \mu_i \sinh y_i, \quad \mathrm{E}_i = \mu_i \cosh y_i, \quad \mu_i = (m_i^2 + p_{i\perp}^2)^{1/2} \qquad (6)$$

using the fact that transverse momenta $p_{i\perp}$ are usually small ($\sim$0.4 Gev/c). Consider $p_{i\perp}$ almost constant, one has $dp_{i//} = \mathrm{E}_i\, dy_i$. Experimental data are usually presented in terms of the following two correlation functions,

$$R^{cd}_{ab}(y_c, y_d, s)$$

$$= \frac{\dfrac{d^2\sigma(a+b\to c+d+X)}{\sigma_{ab}\,dy_c\,dy_d}}{\dfrac{d\sigma(a+b\to c+X)}{\sigma_{ab}\,dy_c}\cdot\dfrac{d\sigma(a+b\to d+X)}{\sigma_{ab}\,dy_d}} - 1 \qquad (7)$$

$$= \frac{\int c^{cd}_{ab}\,d^2p_{c\perp}\,d^2p_{d\perp}}{\int \rho^c_{ab}\,d^2p_{c\perp}\int \rho^d_{ab}\,d^2p_{d\perp}} \qquad (8)$$

noting $dp_{//} \simeq E_i\,dy_i$, and

$$R(\Delta y) = \int R^{cd}_{ab}(y_c, y_d, s)\,\delta(y_c - y_d - \Delta y)\,dy_c\,dy_d\,. \qquad (9)$$

In some cases, the normalization factor σ_{ab} is replaced by the total inelastic cross section σ_{inel}.

By definition, the total cross section is equal to

$$\sigma_{ab} = \frac{1}{v_0}\sum_{n=1}^{\infty}\int d^3p_1\,d^3p_2\ldots d^3p_n\,|\langle i\,|\,\vec{p}_1,\vec{p}_2\ldots\vec{p}_n\rangle|^2 \qquad (10)$$

where v_0 is the relative velocity of particles a and b, $|\vec{p}_1,\vec{p}_2\ldots\vec{p}_n\rangle$ represents a n-particle final state. According to the basic assumption (1) of our model,

$$|\langle i\,|\,\vec{p}_1\vec{p}_2\ldots\vec{p}_n\rangle|^2 = \text{const.}\ I_i\cdot F_f\,.$$

From the definitions of Eqs. (3) and (4), we find

$$\rho^c_{ab}(\vec{p}_c, s)$$

$$= \frac{E_c}{\sigma_{ab}}\frac{1}{v_0}\sum_{n=1}^{\infty}\sum_{i=1}^{n_c}\int d^3p_1\ldots d^3p_i\ldots d^3p_n\,\delta(\vec{p}_i-\vec{p}_c)\cdot|\langle i\,|\,\vec{p}_1,\vec{p}_2\ldots\vec{p}_n\rangle|^2$$

$$= E_c\frac{\sum_{n=1}^{\infty} n_c\int d^3p_1\ldots d^3p_{n-1}\,F_f(\vec{p}_1,\vec{p}_2\ldots\vec{p}_c\ldots\vec{p}_n)}{\sum_{n=1}^{\infty}\int d^3p_1\ldots d^3p_n\,F_f(\vec{p}_1\vec{p}_2\ldots\vec{p}_i\ldots\vec{p}_n)}$$

$$= E_c\sum_{n=1}^{\infty} n_c\,W(n, n_c, \vec{p}_c)$$

where $W(n, n_c, p_c)$ denotes the probability of a c-type particle in $|\vec{p}_c\rangle$ state for a n-particle final state with n_c c-type particles. In terms of statistics average braket,

$$\rho^{c}_{ab}(\vec{p}_c, s) = \mathrm{E}_c\left\langle n_c \cdot \frac{n_c(\vec{p}_c)}{n_c}\right\rangle = \mathrm{E}_c\langle n_c(\vec{p}_c)\rangle \tag{11}$$

where $n_c(\vec{p}_c)$ is the number of c-type particles in $|\vec{p}_c\rangle$ state. Similarly,

$$\begin{aligned}
&\rho^{cd}_{ab}(\vec{p}_c, \vec{p}_d, s) \\
&\quad = \frac{\mathrm{E}_c\,\mathrm{E}_d}{\sigma_{ab}\, v_0} \sum_{n=2}^{\infty} \sum_{i=1}^{n_c} \sum_{j=1}^{n_d} \int d^3p_1 \ldots d^3p_n\, \delta(\vec{p}_i - \vec{p}_c)\, \delta(\vec{p}_j - \vec{p}_d) \\
&\qquad\qquad \cdot |\langle i \mid \vec{p}_1 \ldots \vec{p}_n\rangle|^2 \\
&\quad = \mathrm{E}_c\,\mathrm{E}_d \sum_{n=2}^{\infty} (n_c\, n_d - n_c\, \delta_{cd})\, \mathrm{W}(n, n_c, n_d, \vec{p}_c, \vec{p}_d) \\
&\quad = \mathrm{E}_c\,\mathrm{E}_d \left\langle \left(1 - \frac{\delta_{cd}}{n_c}\right) n_c(\vec{p}_c)\, n_d(\vec{p}_d)\right\rangle .
\end{aligned} \tag{12}$$

From Eqs. (5), (11) and (12), we obtain

$$\begin{aligned}
&C^{cd}_{ab}(\vec{p}_c, \vec{p}_d, s) \\
&\simeq \mathrm{E}_c\,\mathrm{E}_d \Big[\left(1 - \frac{\delta_{cd}}{\langle n_c\rangle}\right) \langle n_c(\vec{p}_c)\, n_d(\vec{p}_c)\rangle \\
&\qquad\qquad - \langle n_c(\vec{p}_c)\rangle \langle n_d(\vec{p}_d)\rangle \Big] .
\end{aligned} \tag{13}$$

In the high energy limit, it is appropriate to take the most probable approximation for the statistical distribution, i.e.,

$$\langle n_i\rangle \simeq n_i^* = \frac{\mathrm{MV}}{e^{\beta \mathrm{E}_i} \mp 1} \qquad \begin{pmatrix} -: \text{ bosons} \\ +: \text{ fermions} \end{pmatrix} \tag{14}$$

where V is the decay volume, and M a normalization constant. Then

$$\begin{aligned}
C^{cd}_{ab} &\simeq \mathrm{E}_c\,\mathrm{E}_d \Big[\left(1 - \frac{\delta_{cd}}{\langle n_c\rangle}\right) \frac{\mathrm{M}^2\,\mathrm{V}^2}{(e^{\beta \mathrm{E}_c} \mp 1)(e^{\beta \mathrm{E}_d} \mp 1)} \\
&\qquad\qquad - \frac{\mathrm{MV}}{e^{\beta \mathrm{E}_c} \mp 1} \cdot \frac{\mathrm{MV}}{e^{\beta \mathrm{E}_d} \mp 1} \\
&\simeq - \frac{\mathrm{E}_c\,\mathrm{E}_d\,\mathrm{M}^2\,\mathrm{V}^2}{(e^{\beta \mathrm{E}_c} \mp 1)(e^{\beta \mathrm{E}_d} \mp 1)} \cdot \frac{\delta_{cd}}{\langle n_c\rangle} .
\end{aligned} \tag{15}$$

The remaining term does not indicate a real correlation between particles, but rather a term reflecting the fact that the same particle can not occupy two different states at the same time. Thus there is no correlation in the high energy limit.

II. STATISTICAL FLUCTUATIONS AND CORRELATIONS

As we have seen, there are no correlations if the most probable approximation of the statistics distribution is taken. We will proceed to study whether small fluctuations around the most probable distribution would lead to correct correlations.

Let $n_{\alpha i}$ be the number of α-type particle in its ith state. For a final state characterized by the occupation numbers $\{n_{\alpha 1}, n_{\beta 2} \ldots\}$, the number of possible combinations is

$$W(\{n_{\alpha i}\}) = \frac{n!}{\prod_{\alpha} n_{\alpha}!} \prod_{\alpha i} w_{\alpha i}, \qquad \sum_{\alpha i} n_{\alpha i} = n \tag{16}$$

where $w_{\alpha i}$ is the number of ways for distributing $n_{\alpha i}$ particles into $g_{\alpha i}$ ith states, that is equal to

$$w_{\alpha i} = \begin{cases} \dfrac{(n_{\alpha i} + g_{\alpha i} - 1)!}{n_{\alpha i}!(g_{\alpha i} - 1)!} & \text{(bosons)} \\ \dfrac{g_{\alpha i}!}{n_{\alpha i}!(g_{\alpha i} - n_{\alpha i})!} & \text{(fermions)}. \end{cases} \tag{17}$$

Naturally, $\{n_{\alpha i}\}$ must satisfy the constraints of energy and momentum conservation,

$$\begin{aligned} \sum_{\alpha i} n_{\alpha i} E_{\alpha i} &= E \\ \sum_{\alpha i} n_{\alpha i} \vec{p}_{\alpha i} &= 0. \end{aligned} \tag{18}$$

in the center-of-mass system.

By the assumption of equal probability for all final states available, the probability for the state $\{n_{\alpha i}\}$ should be

$$P(\{n_{\alpha i}\}) = \frac{W(\{n_{\alpha i}\})}{\sum_{\alpha, i, n} W(\{n_{\alpha i}\})} \tag{19}$$

Assuming the number of particles is large, one can take Stirling's approximations for all factorials. And by the method of Lagrangian multipliers, from Eq. (16), the most probable distributions are found to be

$$n^*_{\alpha i} = \frac{g_{\alpha i}}{\frac{n_{\alpha}}{n} e^{\beta E_{\alpha i} + \vec{\gamma} \cdot \vec{p}_{\alpha i}} \mp 1} \tag{20}$$

where β and $\vec{\tau}$ are constants fixed by conditions (18). Since the constraint

$$\Sigma\, n^*_{\alpha i}\vec{p}_{\alpha i} = \int \rho(m)\, dm \frac{\vec{p}\, V\, d^3p}{\left(\frac{n_\alpha}{n} e^{\beta E + \vec{\tau}\cdot\vec{p}} \mp 1\right)(2\pi)^3} = 0$$

implies $\vec{\tau} = 0$, therefore

$$n^*_{\alpha i} = \frac{g_{\alpha i}}{e^{\beta(E_{\alpha i} - \nu_\alpha)} \mp 1}, \qquad e^{-\nu_\alpha} = n_\alpha/n\,. \tag{21}$$

Next expand $W(\{n_{\alpha i}\})$ around the most probable distributions $\{n^*_{\alpha i}\}$,

$$\begin{aligned}\ln W(\{n_{\alpha i}\}) &= \ln W^* + \sum_{\alpha,i} \frac{\partial}{\partial n_{\alpha i}} \ln W^* \cdot (n_{\alpha i} - n^*_{\alpha i}) \\ &\quad + \frac{1}{2} \sum_{\alpha,\beta,i,j} \frac{\partial^2 \ln W^*}{\partial n_{\alpha i}\, \partial n_{\beta j}} \\ &\quad \cdot (n_{\alpha i} - n^*_{\alpha i})(n_{\beta j} - n^*_{\beta j}) + \ldots \end{aligned} \tag{22}$$

and neglect higher order terms. The Lagrangian multiplier method gives

$$\frac{\partial \ln W^*}{\partial n_{\alpha i}} = \beta E_{\alpha i} + \vec{\tau}\cdot\vec{p}_{\alpha i} \tag{23}$$

Thus the second term of Eq. (22) vanishes for

$$\begin{aligned}&\sum_{\alpha,i} \frac{\partial \ln W^*}{\partial n_{\alpha i}} \cdot (n_{\alpha i} - n^*_{\alpha i}) \\ &\quad = \sum_{\alpha i} (\beta E_{\alpha i} + \vec{\tau}\cdot\vec{p}_{\alpha i})(n_{\alpha i} - n^*_{\alpha i}) = 0\end{aligned}$$

by the conditions (18). Furthermore

$$\begin{aligned}&\frac{\partial^2 \ln W^*}{\partial n_{\alpha i}\, \partial n_{\beta j}} \\ &\quad = \frac{1}{n} - \frac{1}{n_\alpha}\delta_{\alpha\beta} - \left(\frac{1}{n^*_{\alpha i}} - \frac{1}{n^*_{\alpha i} \pm g_{\alpha i}}\right)\delta_{\alpha\beta}\,\delta_{ij}\,.\end{aligned} \tag{24}$$

But

$$\sum_{\alpha,\beta,i,j} \left(\frac{1}{n} - \frac{1}{n_\alpha}\delta_{\alpha\beta}\right)(n_{\alpha i} - n^*_{\alpha i})(n_{\beta j} - n^*_{\beta j}) = 0$$

noting that $\Sigma_i\, n_{\alpha i} = \Sigma_i\, n^*_{\alpha i} = n_\alpha$. It follows that

$$\ln W(\{n_{\alpha i}\}) \simeq \ln W^* - \frac{1}{2}\sum_{\alpha i} A_{\alpha i} x_{\alpha i}^2$$

or

$$W(\{n_{\alpha i}\}) \simeq W^* e^{-1/2 \sum_{\alpha i} A_{\alpha i} x_{\alpha i}^2} \tag{25}$$

where

$$A_{\alpha i} = \frac{1}{n_{\alpha i}^*} - \frac{1}{n_{\alpha i}^* \pm g_{\alpha i}}$$
$$x_{\alpha i} = n_{\alpha i} - n_{\alpha i}^* . \tag{26}$$

For brevity and without confusion, hereafter we shall use a single index (i) in the place of (αi). From Eqs. (19) and (25), the probability for a particular distribution $\{n_i\}$ is given by

$$P(\{n_i\}) \simeq N_0 e^{-1/2 \sum_i A_i x_i^2} \tag{27}$$

where N_0 is a normalization constant. The conditions (18) can be introduced as following

$$P(\{n_i\}) \simeq N_0 e^{-1/2 \sum_i A_i x_i^2} \delta(\sum_i x_i E_i)\, \delta(\sum_i x_i \vec{p}_i) . \tag{28}$$

The statistics average of a quantity f can be written as

$$\langle f \rangle = \sum_{n,i} P(\{n_i\}) \cdot f$$
$$\simeq N_0 \int \prod_i dx_i\, e^{-1/2 \sum_i A_i x_i^2} \delta(\sum_i x_i E_i)\, \delta(\sum_i x_i \vec{p}_i) \tag{29}$$

where $\sum_{n,i}$ has been replaced by integrations of all x_i's over $(-\infty, +\infty)$. This is appropriate if the particle number is large enough and fluctuations are presumably small.

If the kinematic constraints (δ-functions in Eq. (29)) are released, then the fluctuations

$$\langle x_i \rangle = 0$$
$$\langle x_i x_j \rangle = \frac{1}{A_i}\delta_{ij} . \tag{30}$$

In other words,

$$\langle n_i \rangle = n_i^*$$
$$\langle x_i x_j \rangle = \langle n_i n_j \rangle - \langle n_i \rangle \langle n_j \rangle = \frac{1}{A_i}\delta_{ij} . \tag{31}$$

Substituting into Eq. (13), one gets

$$C_{ab}^{cd}(\vec{p}_1, \vec{p}_2, s)$$
$$\simeq -E_1 E_2 \langle n_{c1}\rangle \langle n_{d2}\rangle \frac{\delta_{cd}}{\langle n_c\rangle} + E_1 E_2 \frac{1}{A_{c1}} \delta_{cd}\, \delta_{12}. \tag{32}$$

There is no correlation in this case.

Taking account of the kinematic constraints, we calculate

$$\langle x_j\rangle = N_0 \int \prod_i dx_i\, e^{-1/2 \sum_i A_i x_i^2}\, x_j\, \delta(\sum x_i E_i)\, \delta(\sum x_i \vec{p}_i) \tag{33}$$

with

$$N_0^{-1} \simeq \int \prod_i dx_i\, e^{-1/2 \sum_i A_i x_i^2}\, \delta(\sum x_i E_i)\, \delta(\sum x_i \vec{p}_i).$$

These integrals can be evaluated by replacing the δ-functions by their Fourier integrals. Let

$$\tau \cdot p_i = x p_{ix} + y p_{iy} + z p_{iz} + t E_i$$
$$d\tau = dx\, dy\, dz\, dt$$

then

$$\begin{aligned}\langle x_j\rangle &= N_0 (2\pi)^4 \int e^{-1/2 \sum_i A_i x_i^2}\, x_j\, \delta(\sum_i x_i E_i) \\ &\qquad \cdot \delta(\sum_i x_i \vec{p}_i)\, d\tau \prod_i dx_i \\ &= N_0 (2\pi)^4 \int d\tau \prod_i e^{-1/2(\sqrt{A_i} x_i + \tau \cdot p_i/\sqrt{A_i})^2} \\ &\qquad \cdot e^{-1/2(\tau \cdot p_i)^2/A_i} (1 + x_i \delta_{ij})\, dx_i \\ &= -N_0 (2\pi)^4 \prod_i \sqrt{\frac{2\pi}{A_i}} \int \frac{i(\tau \cdot p_j)}{A_j} e^{-1/2 \sum_i (\tau \cdot p_i)^2/A_i}\, d\tau \\ &= 0. \end{aligned} \tag{34}$$

Thus $\langle n_i\rangle = n_i^*$ and $\langle x_i x_j\rangle = \langle n_i n_j\rangle - \langle n_i\rangle\langle n_j\rangle$. Similarly,

$$\langle x_i x_j\rangle = -\frac{1}{A_i A_j} \sum_{\mu,\nu=1}^{4} p_{i\mu} p_{j\nu} \overline{\tau_\mu \tau_\nu} + \frac{1}{A_i} \delta_{cd}\, \delta(\vec{p}_i - \vec{p}_j) \tag{35}$$

where

$$\overline{\tau_\mu \tau_\nu} = \frac{\int e^{-1/2 \sum_{\mu\nu} a_{\mu\nu} \tau_\mu \tau_\nu}\, \tau_\mu \tau_\nu\, d\tau}{\int e^{-1/2 \sum a_{\mu\nu} \tau_\mu \tau_\nu}\, d\tau} \tag{36}$$

and

$$a_{\mu\nu} = \sum_i \frac{p_{i\mu}\, p_{i\nu}}{A_i} = \frac{V}{(2\pi)^3} \int \rho(m)\, dm\, \frac{p_{i\mu}\, p_{i\nu}}{A_i}\, d^3 p_i$$

$$= \sum_i \frac{p_{i\mu}^2}{A_i}\, \delta_{\mu\nu} \tag{37}$$

since A_i depends on p_i^2 only. The last term of Eq. (35) represents the standard deviation of n_i from n_i^*. The integration of Eq. (36) can be done by routine procedure[2], the result gives

$$\overline{\tau_\mu \tau_\nu} = a_{\mu\nu}^{-1} = \frac{1}{a_{\mu\mu}}\, \delta_{\mu\nu}\,. \tag{38}$$

Therefore

$$\langle x_i\, x_j \rangle = -\frac{1}{A_i A_j} \sum_{\mu=1}^{4} \frac{p_{i\mu}\, p_{j\mu}}{a_{\mu\mu}} + \frac{1}{A_i}\, \delta_{ij}\, \delta(\vec{p}_i - \vec{p}_j) \tag{39}$$

and

$$C_{ab}^{cd}(\vec{p}_1, \vec{p}_2, s)$$

$$\simeq E_1 E_2 \Big[\Big(1 - \frac{\delta_{cd}}{\langle n_c \rangle}\Big) \Big(\frac{1}{A_1}\, \delta_{cd}\, \delta(\vec{p}_1 - \vec{p}_2)$$

$$- \frac{1}{A_1 A_2} \sum_{\mu=1}^{4} \frac{p_{1\mu}\, p_{2\mu}}{a_{\mu\mu}} \Big) - \langle n_{c1} \rangle \langle n_{d2} \rangle \frac{\delta_{cd}}{\langle n_c \rangle} \Big]. \tag{40}$$

III. TWO-PARTICLE CORRELATIONS

For the calculation of two-particle correlations, first we estimate related constants with the approximation in the high energy limit. Eqs. (20) and (26) lead to

$$A_i = \frac{1}{n_i^*} - \frac{1}{n_i^* \pm g_i} = \frac{1}{n_i^*} \left(1 \mp e^{-\beta(E_i - \nu_i)}\right)$$

$$= \frac{4}{g_i} \begin{pmatrix} \sinh^2 \frac{1}{2}\beta(E_i - \nu_i) \\ \cosh^2 \frac{1}{2}\beta(E_i - \nu_i) \end{pmatrix} \geq 0$$

$$\simeq \frac{1}{n_i^*} \simeq e^{+\beta E_i} \tag{41}$$

as $E \to \infty$. By the definition of Eq. (37),

$$a_{11} = a_{22} = a_{33} = \frac{1}{3} \sum_i \frac{p_i^2}{A_i} \simeq \frac{1}{3} \sum_i n_i^*\, p_i^2 \tag{42}$$

noting that A_i depends on p_i^2 only, and

$$\begin{aligned} a_{44} &= \sum_i \frac{E_i^2}{A_i} \simeq \sum_i n_i^* E_i^2 \\ &\simeq \int \rho(m)\, dm\, \varepsilon^2\, e^{-\beta\varepsilon}\, \frac{V\, d^3p}{(2\pi)^3} \\ &\simeq -\frac{\partial}{\partial\beta} \int \rho(m)\, dm\, \varepsilon\, e^{-\beta\varepsilon}\, \frac{V\, d^3p}{(2\pi)^3} \\ &\simeq -\frac{\partial E}{\partial\beta} \end{aligned} \tag{43}$$

where E is the total energy. Furthermore

$$\begin{aligned} & a_{44} - (a_{11} + a_{22} + a_{44}) \\ &= \sum_i \frac{m_i^2}{A_i} \simeq \sum_i m_i^2 n_i^* \\ &\simeq \int cm^{-5/2} e^{bm} \cdot m^2\, e^{-\beta\varepsilon}\, dm\, \frac{V\, d^3p}{(2\pi)^3} \\ &\simeq \frac{\partial^2}{\partial b^2} \int cm^{-5/2} e^{bm}\, e^{-\beta\varepsilon}\, dm\, \frac{V\, d^3p}{(2\pi)^3} \\ &\simeq \frac{\partial^2 \bar{n}}{\partial b^2} \end{aligned} \tag{44}$$

where $\bar{n}$ is the average multiplicity. Both E and $\bar{n}$ have been calculated and given in Ref. 1. As $E \to \infty$, or $x = (\beta - b)\, m_0 \to 0$,

$$\begin{aligned} E &\simeq \frac{cV}{(2\pi\beta)^{3/2}}\, m_0 \left[\frac{e^{-x}}{x} + \frac{27}{8\beta m_0} E_i(x)\right] \\ \bar{n} &\simeq \frac{cV}{(2\pi\beta)^{3/2}} [-\ln x + \gamma]\,. \end{aligned} \tag{45}$$

By derivation, we get

$$a_{44} \simeq E \cdot \frac{m_0}{x} \simeq \frac{E}{\beta - b} \propto E^2 \tag{46}$$

$$a_{11} = a_{22} = a_{33} \simeq \frac{-1}{3} \left(\frac{\partial E}{\partial\beta} - \frac{\partial^2 \bar{n}}{\partial b^2}\right) \simeq \frac{13E}{8\beta} \propto E\,. \tag{47}$$

As energy increases, $a_{44} \gg a_{11} \ldots$, the contribution of the a_{44} terms to $\langle x_i\, x_j \rangle$ becomes less important. In other words, the energy conservation constraint becomes less important to two-particle correlations. As $E \to \infty$, $a_{\mu\mu} \to \infty$ and so $\langle x_i\, x_j \rangle \to 0$. There are no correlations in the high energy limit.

In our statistics model, the distribution in the CM system is isotropic in momentum space, first we will define and investigate a momentum symmetric correlation function

$$R(\Delta p) = \frac{\int \frac{E_1 E_2 d^6\sigma(a+b\to c+d+X)}{\sigma_{ab} d^3p_1 d^3p_2} \delta(\vec{p}_1-\vec{p}_2-\Delta\vec{p}) d^3p_1 d^3p_2}{\int \frac{E_1 d^3\sigma(a+b\to c+X) E_2 d^3\sigma(a+b\to d+X)}{\sigma_{ab} d^3p_1 \sigma_{ab} d^3p_2} \delta(\vec{p}_1-\vec{p}_2-\Delta\vec{p}) d^3p_1 d^3p_2} - 1$$

$$= \frac{1}{I_0} \int C^{cd}_{ab}(\vec{p}_1, \vec{p}_2, s)\, \delta(\vec{p}_1 - \vec{p}_2 - \Delta\vec{p})\, d^3p_1 d^3p_2 \tag{48}$$

with

$$I_0 = \int E_1 E_2 \langle n_1\rangle \langle n_2\rangle \delta(\vec{p}_1 - \vec{p}_2 - \Delta\vec{p})\, d^3p_1 d^3p_2 \tag{49}$$

Take the approximation,

$$\langle n_i\rangle \simeq \frac{n_\alpha}{n} e^{-\beta E_i}$$
$$E_i \simeq m_i\left[1 + \frac{p_i^2}{2m_i^2} + O(p_i^4)\right] \tag{50}$$

recalling that p_i^2 in the CM system is usually small ($\sim$0.4 Gev/c), after tedious but straightforward calculation, we find

$$I_0 \simeq \left(\frac{n_c n_d}{n^2}\right)\frac{m_1 m_2 \sqrt{\pi^3}}{\zeta^3} e^{-\beta(m_1+m_2)}\left[\left(1 + \frac{3(m_1+m_2)}{2\beta m_1 m_2} - \frac{3}{\beta(m_1+m_2)}\right) + \frac{\Delta p^2}{(m_1+m_2)^2}\right] e^{-\Delta p^2/\xi^2},$$
$$\zeta^2 = \frac{\beta(m_1+m_2)}{2m_1 m_2}, \quad \xi^2 = \frac{2(m_1+m_2)}{\beta} \tag{51}$$

$$I_1 = \int E_1 E_2 \frac{1}{A_1 A_2}\left(\frac{\vec{p}_1\cdot\vec{p}_2}{a_{11}} + \frac{E_1 E_2}{a_{44}}\right)\delta(\vec{p}_1 - \vec{p}_2 - \Delta\vec{p})\, d^3p_1 d^3p_2$$
$$\simeq \frac{n_c n_d}{n^2}\frac{\sqrt{\pi^3}}{\zeta^3} m_1 m_2 e^{-\beta(m_1+m_2)}\left\{\left[\frac{1}{a_{11}}\frac{3m_1 m_2}{\beta(m_1+m_2)} + \frac{1}{a_{44}}\left(m_1 m_2 + \frac{3(m_1^2+m_2^2)}{\beta(m_1+m_2)}\right)\right] + \frac{m_1 m_2}{(m_1+m_2)^2}\left(\frac{2}{a_{44}} - \frac{1}{a_{11}}\right)\Delta p^2\right\} e^{-\Delta p^2/\xi^2} \tag{52}$$

$$I_2 = \int E_1 E_2 \frac{1}{A_1}\delta(\vec{p}_1 - \vec{p}_2)\,\delta(\vec{p}_1 - \vec{p}_2 - \Delta\vec{p})\, d^3p_1 d^3p_2$$
$$= \frac{n_c}{n} m_1^2 e^{-\beta m_1}\sqrt{\pi^3}\frac{1}{\zeta_1^3}\left(1 + \frac{3}{\beta m_1}\right)\delta(\Delta\vec{p}), \qquad \zeta_1^2 = \frac{\beta}{2m_1} \tag{53}$$

and

$$\bar{R}(\Delta p) = \left(1 - \frac{\delta_{cd}}{\langle n_c \rangle}\right)\left[\frac{I_2 \delta_{cd} - I_1}{I_0}\right] - \frac{\delta_{cd}}{\langle n_c \rangle} . \tag{54}$$

For like particles, $m_1 = m_2 = m$,

$$\bar{R}(\Delta p) \simeq \sqrt{8}\ \frac{n}{n_c} e^{\beta m}\left(1 + \frac{3}{2\beta m} - \frac{\Delta p^2}{4m^2}\right)\delta(\Delta \vec{p}) - a\left[1 - \left(1 + \frac{2\beta m}{3}\right)\frac{\Delta p^2}{4m^2}\right] \tag{55}$$

$$a = \frac{m^2}{(2\beta m + 3)}\left[\frac{3}{a_{11}} + \frac{2\beta m + 6}{a_{44}}\right]$$

after negleting $\delta_{cd}/\langle n_c \rangle$. The correlation length estimated from above equation is about

$$2 \cdot \Delta p_{1/2} \simeq 4m . \tag{56}$$

For direct comparison with experiments[3,4], we proceed to calculate the correlation functions $R^{cd}_{ab}(y_1, y_2, s)$ and $R(\Delta y)$. In similar ways, we obtain

$$I_0' = \int E_1 E_2 \langle n_1 \rangle \langle n_2 \rangle d^2 p_{1\perp} d^2 p_{2\perp} \tag{57}$$

$$\simeq \int \mu_1 \mu_2 \cosh y_1 \cosh y_2\, e^{-\beta(\mu_1 \cosh y_1 + \mu_2 \cosh y_2)} (2\pi)^2 p_{1\perp}\, dp_{1\perp}\, p_{2\perp}\, dp_{2\perp}$$

$$\simeq (2\pi)^2 \int \mu_1 \mu_2 \cosh y_1 \cosh y_2\, e^{-\beta(\mu_1 \cosh y_1 + \mu_2 \cosh y_2)}\, \mu_1\, d\mu_1\, \mu_2\, d\mu_2$$

$$\simeq (2\pi)^2 \left(\frac{m_1 m_2}{\beta}\right)^2 \cosh y_1 \cosh y_2 \cdot e^{-(t_1 + t_2)}(1 + 2t_1^{-1} + 2t_1^{-2})(1 + 2t_2^{-1} + 2t_2^{-2}) ,$$

$$t_i = \beta m_i \cosh y_i \tag{58}$$

$$I_1' = \int E_1 E_2 \frac{1}{A_1 A_2}\left(\frac{\vec{p}_{1\perp} \cdot \vec{p}_{2\perp} + p_{1//}\, p_{2//}}{a_{11}} + \frac{E_1 E_2}{a_{44}}\right) d^2 p_{1\perp}\, d^2 p_{2\perp} \tag{59}$$

$$\simeq (2\pi)^2 \int \mu_1^3 \mu_2^3 \cosh y_1 \cosh y_2 \cdot e^{-\beta(\mu_1 \cosh y_1 + \mu_2 \cosh y_2)}\left(\frac{\sinh y_1 \sinh y_2}{a_{11}} + \frac{\cosh y_1 \cosh y_2}{a_{44}}\right) d\mu_1\, d\mu_2$$

$$\simeq \left(\frac{2\pi}{\beta}\right)^2 m_1^3 m_2^3 \cosh y_1 \cosh y_2\left[\frac{\sinh y_1 \sinh y_2}{a_{11}} + \frac{\cosh y_1 \cosh y_2}{a_{44}}\right] \cdot e^{-(t_1 + t_2)}(1 + 3t_1^{-1} + 6t_1^{-2} + 6t_1^{-3})(1 + 3t_1^{-1} + 6t_1^{-2} + 6t_1^{-3}) \tag{60}$$

$$I_2' = \delta_{cd} \int E_1 E_2 \frac{1}{A_1} \delta(\vec{p}_1 - \vec{p}_2)\, d^2 p_{1\perp}\, d^2 p_{2\perp} \tag{61}$$

$$\simeq \delta_{cd}\, \delta(p_{1//} - p_{2//}) \int E_1^2 e^{-\beta E_1} d^2 p_{1\perp}$$

$$\simeq \delta_{cd}\, \delta(y_1 - y_2) \frac{2\pi m_1^2}{\beta} e^{-t_1}(1 + 3t_1^{-1} + 6t_1^{-2} + 6t_1^{-3}) . \tag{62}$$

Substitute Eqs. (58)–(62) into Eqs. (8) and (39), we obtain

$$R_{ab}^{cd}(y_1, y_2, s)$$

$$= \left(1 - \frac{\delta_{cd}}{\langle n_c \rangle}\right) \frac{I_2' - I_1'}{I_0'} - \frac{\delta_{cd}}{\langle n_c \rangle} \tag{63}$$

$$\simeq \left(1 - \frac{\delta_{cd}}{\langle n_c \rangle}\right)\left[\frac{\beta}{2\pi m_1^2 \cosh^2 y_1} e^{+t_1} \delta_{cd}\, \delta(y_1 - y_2)\right.$$

$$\left. - m_1 m_2 \left[\frac{\sinh y_1 \sinh y_2}{a_{11}} + \frac{\cosh y_1 \cosh y_2}{a_{44}}\right](1 + t_1^{-1} + t_2^{-1})\right]$$

$$- \frac{\delta_{cd}}{\langle n_c \rangle} \tag{64}$$

after neglecting higher order terms of t_i inverses.

By definition,

$$R(\Delta y) = \int R_{ab}^{cd}(y_1, y_2, s)\, \delta(y_1 - y_2 - \Delta y)\, dy_1\, dy_2 \tag{65}$$

$$= \int R_{ab}^{cd}(y_2 + \Delta y, y_2, s)\, dy_2 \tag{66}$$

The integral diverges if y_2 is integrated from $-\infty$ to $+\infty$. In fact, the limits of integration should be determined by energy and momentum conservation,

$$\begin{aligned} E_1 + E_2 &= m_1 \cosh y_1 + m_2 \cosh y_2 \\ &= m_1 \cosh(y_2 + \Delta y) + m_2 \cosh y_2 \leq E \\ \sum_i \mu_i \sinh y_i &= 0 . \end{aligned} \tag{67}$$

The solution of Eq. (67) is estimated to be

$$\begin{aligned} y_{max} - y_{min} &\simeq 2 \cosh^{-1} \frac{E}{2C} \\ &\xrightarrow[m_1 = m_2]{} 2 \ln E - 2 \ln 2m_1 \cosh \frac{\Delta y}{2} \\ y_{max} + y_{min} &\simeq -2d \xrightarrow[m_1 = m_2]{} -\Delta y \end{aligned} \tag{68}$$

where

$$C = (m_1^2 + m_2^2 + 2m_1 m_2 \cosh \Delta y)^{1/2} \xrightarrow[m_1 = m_2]{} 2m_1 \cosh \frac{\Delta y}{2}$$
$$d = \tanh^{-1} \frac{\sinh \Delta y}{\frac{m_2}{m_1} + \cosh \Delta y} \xrightarrow[m_1 = m_2]{} \frac{\Delta y}{2} . \tag{69}$$

Finally the integral of Eq. (66) is evaluated

$$\begin{aligned} R(\Delta y) \simeq & \left(1 - \frac{\delta_{cd}}{\langle n_c \rangle}\right) \left\{ \frac{16\, e^{\beta(E/4)}}{\pi E^4} \delta_{cd}\, \delta(\Delta y) \right. \\ & - m_1 m_2 \left[\frac{1}{2a_{11}} (\cosh (y_{max} + y_{min} + \Delta y) \sinh (y_{max} - y_{min}) \right. \\ & - (y_{max} - y_{min}) \cosh \Delta y) \\ & + \frac{1}{2a_{44}} (\cosh (y_{max} + y_{min} + \Delta y) \cosh (y_{max} - y_{min}) \\ & \left. \left. + (y_{max} - y_{min}) \cosh \Delta y) \right] \right\} \\ & - \frac{\delta_{cd}}{\langle n_c \rangle} (y_{max} - y_{min}) \\ \simeq & \left(1 - \frac{\delta_{cd}}{\langle n_c \rangle}\right) \left\{ \frac{16}{\pi E^4} e^{\beta E/4} \delta_{cd}\, \delta(\Delta y) \right. \\ & - m_1 m_2 \left[\frac{E^2}{16 m^2 \cosh^2 (\Delta y/2)} \left(\frac{1}{a_{11}} \left(1 - \frac{8m^2 \cosh^2 (\Delta y/2)}{E^2}\right) \right. \right. \\ & + \frac{1}{a_{44}} \left. \left(1 - \frac{16 m^2 \cosh^2 (\Delta y/2)}{E^2}\right)^{1/2} \right) \\ & \left. \left. - \cosh^{-1} \frac{E}{4m \cosh (\Delta y/2)} \cdot \cosh \Delta y \left(\frac{1}{a_{11}} - \frac{1}{a_{44}} \right) \right] \right\} \\ & - 2 \cosh^{-1} \frac{E}{4m \cosh (\Delta y/2)} \cdot \frac{\delta_{cd}}{\langle n_c \rangle} . \end{aligned} \tag{70}$$

IV. DISCUSSION AND CONCLUSION

1. The correlations calculated mainly come from kinematic constraints of energy and momentum conservation, and vanish in the energy limit. The correlation length of Δp is about $4m$. These results are compatable with experiments.

2. The first term of Eqs. (64) and (70) represents the standard deviation of n_i. Terms with the δ_{cd} factor exist because one particle can not simultaneously occupy two different states. They do not represent real correlations.

3. From Eqs. (37), (39) and (41), we find that $a_{\mu\mu} > 0$, and $A_i > 0$, thus the correlation $\langle x_i x_j \rangle$ is always negative except the unrelated last term.

4. Eqs. (64) and (70) are statistical average correlations. For $\pi\pi$ and KK correlations, the degeneracy factor g_i of such low mass states, shown in Eq. (2), must be taken into account. The effect can be estimated by consideration of isospin conservation[5].

5. Hsu[5] has made computer calculations of $R(\Delta y)$, considering only energy conservation, i.e., keeping only a_{44} terms. The results are found to be in good consistancy with experiments[3,4], except their signs are different. Table 1 shows the result of $R(\Delta y)$ at $\Delta y = 0$ and $E = 200$ Gev. Since the correlations R_{expt} used in Refs. 3–4 are normalized by σ_{inel} instead of σ_{ab}, an additional factor $\sigma_{inel}/\sigma_{ab}$ ($\sim$0.7) should multiply R_{theo} in Table 1. This makes the results even better. By inspecting the function dependence of Eq. (70), we find that the inclusion of a_{11} terms would lead to similar results, although these terms dominate as energy increases.

Table 1. Correlations $R(\Delta y = 0)$ at 200 Gev

	$R_{theo}(0)$	$R_{expt}(0)$
$\pi^- \pi^-$	−0.53	0.3
$\pi^+ \pi^-$	−1.208	0.65
$\pi^+ \pi^+$	−0.494	0.3
$K_s^0 K_s^0$	−3.143	2.33±0.54

REFERENCES

(1) Chen, J., *Fu Jen Studies* **10**, 25 (1976).
(2) Landau, L. and E. Lifshitz, *Statistics Physics*, §110.
(3) Biswas, N. *et al.*, *Phys. Rev. Lett.* **35**, 1059 (1975).
(4) Harris, R. *et al.*, *Phys. Rev.* **D18**, 92 (1978).
(5) Hsu, C., *MS Thesis*, Physics Dept., Fu Jen Univ. (1979, unpublished).
(6) Foa, L., *Phys. Lett.* **22C**, 1 (1975).
(7) Slansky, R., *Phys. Lett.* **11C**, 99 (1975).

"It is the so-called '*scientific revolution*', popularly associated with the sixteenth and seventeenth centuries, but reaching back in an unmistakably continuous line to a period much earlier still. Since that revolution overturned the authority in science not only of the middle ages but of the ancient world—since it ended not only in the eclipse of scholastic philosophy but in the destruction of Aristotelian physics—it outshined everything since the rise of Christianity and reduces the Renaissance to the rank of mere episodes..."

HERBERT BUTTERFIELD
The origin of modern science

REALIZATION OF STOCHASTIC LINEAR CONSTANT SYSTEMS USING LUENBERGER'S CANONICAL FORMS

ZUON-HUA LUO

ABSTRACT

This paper describes a new algorithm for realizing the stochastic linear constant system from the output covariance function. This algorithm makes use of the two Luenberger's canonical forms to symplify the equations relating the system matrices to the output covariance function. It is shown that the computational efforts required are considerably reduced and the set of equivalent system noise covariances in the sense that they all lead to the same output covariance function is explicitly described.

1. INTRODUCTION

The stochastic realization problem has long been studied in the engineering literature[1-11]. Some papers are mainly concerned with parameter estimation[1-4], while others tend to take advantage of the system structure and require less computational effort[5-11]. This paper gives a new algorithm for the stochastic realization and meanwhile solves an important problem which arises in the realization.

For the state-space representation of stochastic linear constant systems, two different system noise covariances Q's may lead to the same output covariance function C_i. Then the question is: Under what conditions can this happen? In this paper it will be shown that the answer is: When the system matrices are in the generalized companion form[12], two different Q's may lead to the same C_i if and only if the two Q's have the same block diagonal sums.

The algorithm developed in this paper for the stochastic realization is a two-step procedure based on minimal realization and identification of Q. A minimal realization in Luenberger's first canonical form is first constructed from the output covariance function C_i. Then this realization is transformed to Luenberger's second

canonical form. The transformation is easy since the parameters of the second form can be directly computed from the parameters of the first form[17] and the nonsingular matrix required to make the transformation can be also easily obtained from the first canonical form[18]. The next step is to convert the second canonical form to the generalized companion form for identifying Q. This conversion simply involves the rearrangement and augmentation of the system states. After the generalized companion form has been obtained, it is used to simplify the covariance equation and to identify the Q.

2. LUENBERGER'S CANONICAL FORMS

In this section we derive Luenberger's canonical forms in a way quite different from the original derivation in his paper[13]. We consider a linear constant system described by a difference equation of the form

$$x(t+1) = \mathrm{F}x(t) + \mathrm{G}u(t) \tag{1}$$

where $x(t)$ is an $n \times 1$ state vector, $u(t)$ is an $m \times 1$ input vector, and F, G are respectively $n \times n$ and $n \times m$ constant matrices. It will be assumed that the pair (F, G) is completely controllable and G has full rank, i.e.,

$$\text{rank}\,[\mathrm{G}\ \mathrm{FG} \ldots \mathrm{F}^{n-1}\mathrm{G}] = n \quad \text{and} \quad \text{rank}\,\mathrm{G} = m\,.$$

Given the pair (F, G) we have the following vectors:

$$g_1 \ldots g_m \ldots \mathrm{F}^{n-1} g_1 \ldots \mathrm{F}^{n-1} g_m \tag{2}$$

where g_i is the ith column of G. Since (F, G) is completely controllable, it is always possible to select n linearly independent vectors from (2). Selecting the first n linearly independent vectors, we obtain

$$g_1 \ldots \mathrm{F}^{\nu_1 - 1} g_1 \ldots g_m \ldots \mathrm{F}^{\nu_m - 1} g_m \tag{3}$$

where the integers $\nu_1, \ldots, \nu_m$ are known as the Kronecker indices of (F, G)[14-16].

From the selection procedure just stated we have the following linear dependence equations:

$$F^{\nu_j} g_j = \sum_{i=1}^{m} \sum_{k=1}^{\min(\nu_i, \nu_j)} a_{ijk} F^{k-1} g_i + \sum_{\substack{i=1 \\ \nu_j < \nu_i}}^{j-1} c_{ij} F^{\nu_j} g_i \qquad j = 1, \ldots, m \qquad (4)$$

where the last sum is taken over those i's $(i = 1, \ldots, j-1)$ for which $\nu_j < \nu_i$. We notice that the coefficients a_{ijk}'s and c_{ij}'s, together with the Kronecker indices ν_i's, form a complete set of invariants for (F, G)[14]. We construct a nonsingular matrix of the form

$$T_1 = [g_1 \ldots F^{\nu_1 - 1} g_1 \ldots g_m \ldots F^{\nu_m - 1} g_m]. \qquad (5)$$

Then it is easily shown by direct computation that (F, G) can be transformed to the form

$$F^* = T_1^{-1} F T_1 = \begin{bmatrix} A_{11} & A_{12} & \ldots & A_{1m} \\ A_{21} & A_{22} & \ldots & A_{2m} \\ \vdots & & & \\ A_{m1} & A_{m2} & \ldots & A_{mm} \end{bmatrix} \qquad (6)$$

$$G^* = T_1^{-1} G = [g_1^* \quad g_2^* \ldots g_m^*] \qquad (7)$$

where A_{ii} is a $\nu_i \times \nu_i$ companion matrix, $A_{ij} (i \neq j)$ is a $\nu_i \times \nu_j$ matrix, and g_i^* is an $n \times 1$ column vector, given by

$$A_{ii} = [e_2 \quad e_3 \ldots e_{\nu_i} \quad a_{ii}]$$

$$A_{ij} = [0 \quad 0 \ldots 0 \quad a_{ij}]$$

$$g_i^* = e_{\nu_1 + \nu_2 + \cdots + \nu_{i-1} + 1}$$

where

e_i = the unit vector with a 1 in the ith position

$$a'_{ii} = [a_{ii1} \quad a_{ii2} \ldots a_{ii\nu_i}]$$

$$a'_{ij} = [a_{ij1} \quad a_{ij2} \ldots a_{ij\nu_i}] \qquad \text{if } \nu_i \leq \nu_j$$

$$a'_{ij} = [a_{ij1} \quad a_{ij2} \ldots a_{ij\nu_j} \quad c_{ij} \quad 0 \ldots 0] \qquad \text{if } \nu_j < \nu_i$$

The pair (F*, G*) is known as Luenberger's first canonical form of (F, G).

Luenberger's second canonical form of (F, G) may be derived by first forming a nonsingular matrix of the form

$$T_2 = [s_{11} \dots s_{1\nu_1} \dots s_{m1} \dots s_{m\nu_m}], \tag{8}$$

where

$$\begin{cases} s_{j\nu_j} = g_j - \sum\limits_{\substack{i=1 \\ \nu_j < \nu_i}}^{j=1} c_{ij}\, g_i & j = 1, 2, \dots, m \\ s_{j(\nu_j-1)} = \mathrm{F}s_{j\nu_j} - \sum\limits_{\nu_j \le \nu_i}^{m} a_{ij\nu_j}\, g_i \\ \quad \vdots \\ s_{j1} = \mathrm{F}s_{j2} - \sum\limits_{2 \le \nu_i}^{m} a_{ij2}\, g_i . \end{cases}$$

Then it can be shown[18] that (F, G) can be transformed to the form

$$\mathrm{F}^{**} = \mathrm{T}_2^{-1}\mathrm{F}\mathrm{T}_2 = \begin{bmatrix} \mathrm{B}_{11} & \mathrm{B}_{12} \dots \mathrm{B}_{1m} \\ \mathrm{B}_{21} & \mathrm{B}_{22} \dots \mathrm{B}_{2m} \\ \vdots & \\ \mathrm{B}_{m1} & \mathrm{B}_{m2} \dots \mathrm{B}_{mm} \end{bmatrix} \tag{9}$$

$$\mathrm{G}^{**} = \mathrm{T}_2^{-1}\mathrm{G} = [g_1^{**} \quad g_2^{**} \dots g_m^{**}], \tag{10}$$

where B_{jj} is a $\nu_j \times \nu_j$ companion matrix, $\mathrm{B}_{ij}(i \neq j)$ is a $\nu_i \times \nu_j$ matrix, and g_j^{**} is an $n \times 1$ column vector, given by

$$\mathrm{B}'_{jj} = [e_2 \quad e_3 \dots e_{\nu_j} \quad b_{jj}]$$

$$\mathrm{B}'_{ij} = [0 \quad 0 \dots 0 \quad b_{ij}]$$

$$g_j^{**} = e_{\nu_1+\dots+\nu_j} + \sum_{\substack{i=1 \\ \nu_j < \nu_i}}^{j-1} d_{ij}\, e_{\nu_1+\dots+\nu_i}$$

where

$$b'_{jj} = [b_{jj1} \quad b_{jj2} \dots b_{jj\nu_j}]$$

$$b'_{ij} = [b_{ij1} \quad b_{ij2} \dots b_{ij\nu_j}] \qquad \text{if} \quad \nu_j \le \nu_i$$

$$b'_{ij} = [b_{ij1} \quad b_{ij2} \dots b_{ij\nu_i} \quad 0 \dots 0] \qquad \text{if} \quad \nu_i < \nu_j$$

The pair (F**, G**) is known as Luenberger's second canonical form of (F, G). It is noted here that the elements b_{ijk}'s and d_{ij}'s, together with the Kronecker indices ν_i's, form a second complete

set of invariants for (F, G). Furthermore, this set of invariants can be directly computed from the first set of invariants by the following recursive formulas given in a previous paper[17]

$$\text{a)}\quad d_{ij} = c_{ij} + \sum_{\substack{r=i+1 \\ \nu_j < \nu_r < \nu_i}}^{j-1} d_{ir}\, c_{rj} \qquad \begin{matrix} i = 1, \ldots, m-1; \\ j = i+1, \ldots, m \\ \text{with } \nu_j < \nu_i \end{matrix} \tag{11}$$

where d_{ij} is computed after $d_{i(i+1)}, d_{i(i+2)}, \ldots, d_{i(j-1)}$ have been computed.

$$\text{b)}\quad b_{ijk} = a_{ijk} + \sum_{\substack{r=i+1 \\ k \le \nu_r < \nu_i}}^{m} d_{ir}\, a_{rjk} \qquad \begin{matrix} i, j = 1, \ldots, m; \\ k = 1, \ldots, \min(\nu_i, \nu_j). \end{matrix} \tag{12}$$

It is noted here that the nonsingular matrix T_2 was first given by Popov[14] in his study of the invariants a_{ijk}'s and c_{ij}'s. Later Chan and Wang[18] showed that it can be used to derive the second form. This derivation of the second form is a generalization of the well known method for the single-input case[19].

To determine the second form from the first form, however, we need not compute the matrix T_2. It suffices to calculate the invariants b_{ijk}'s and d_{ij}'s from the invariants a_{ijk}'s and c_{ij}'s by (11) and (12).

Now suppose that we are given a triple (F, G, H) where H is the output matrix of the system (1). If we are required to compute another triple $(F^{**}, G^{**}, H^{**}) = (T_2^{-1}FT_2, T_2^{-1}G, HT_2)$, we have to compute the matrix T_2 in order to determine the new output matrix $H^{**} = HT_2$. This will be discussed in detail in the next section.

3. MINIMAL REALIZATION

Suppose that the system (1) considered in the last section has p outputs, then it can be expressed as

$$\begin{aligned} x(t+1) &= Fx(t) + Gu(t) \\ y(t) &= Hx(t) \end{aligned} \tag{13}$$

where H is a $p \times n$ constant matrix. Let $Y_0, Y_1, \ldots$ be the impulse response sequence of (13), then we have

$$Y_i = HF^i G \qquad i = 0, 1, \ldots \tag{14}$$

The realization problem is this: Given an infinite sequence of $p \times m$ matrices $Y_0, Y_1, \ldots$, find a triple (F, G, H) such that the equation (14) holds. A realization (F, G, H) is said to be minimal if the size of the matrix F is minimal. Clearly, for any two minimal realizations (F_1, G_1, H_1) and (F_2, G_2, H_2) there exists a nonsingular matrix T such that $(F_2, G_2, H_2) = (T^{-1}F_1T, T^{-1}G_1, H_1T)$. Further, a minimal realization is both completely controllable and completely observable[20].

To determine a minimal realization (F, G, H) from the sequence $Y_0, Y_1, \ldots$, any one of the realizatian algorithms given in[21-25] can be used. In this section, however, we shall describe an algorithm which leads to minimal realizations in Luenberger's canonical forms.

Consider the Hankel matrix

$$T(0, n-1) = \begin{bmatrix} Y_0 & Y_1 \ldots Y_{n-1} \\ Y_1 & Y_2 \ldots Y_n \\ \vdots & \\ Y_{n-1} & Y_n \ldots Y_{2n-2} \end{bmatrix}$$

where the dimension n is determined according to the formula

$$n = \max_i \operatorname{rank} T(0, i).$$

The Hankel matrix $T(0, n-1)$ can be factored as the product of the observability matrix and the controllability matrix of the system

$$T(0, n-1) = \begin{bmatrix} H \\ HF \\ \vdots \\ HF^{n-1} \end{bmatrix} [G \; FG \ldots F^{n-1}G].$$

Obviously the Hankel matrix $T(0, n-1)$ has rank n and its column dependence relations are equivalent to those of the controllability matrix. Thus premultiplying the equation (4) by the observability matrix S, we obtain the following column dependence relations for $T(0, n-1)$

$$SF^{\nu_j} g_j = \sum_{i=1}^{m} \sum_{k=1}^{\min(\nu_i, \nu_j)} a_{ijk} SF^{k-1} g_i + \sum_{\substack{i=1 \\ \nu_j < \nu_i}}^{j-1} c_{ij} SF^{\nu_j} g_i$$

$$j = 1, \ldots, m \quad (15)$$

In view of (15), we note that the Kronecker indices ν_i's of (F, G) can be determined by examining the column dependence relations in $T(0, n-1)$. Also the elements a_{ijk}'s and c_{ij}'s of the first canonical form (F*, G*) can be obtained by solving (15).

It now remains to compute the corresponding output matrix H*. Let H* be written in terms of its columns as

$$H^* = [h_{11}^* \ldots h_{1\nu_1}^* \ldots h_{m1}^* \ldots h_{m\nu_m}^*].$$

Then it is easily shown by simple matrix operations that

$$h_{ij}^* = H^*(F^*)^{j-1} g_i^* = HF^{j-1} g_i$$

which is the ith column of Y_{j-1}. This completes the minimal realization in the first canonical form.

If it is required to obtain a minimal realization in the second canonical form, we may first use the preceding algorithm to obtain a minimal realization in the first canonical form and then transform it to the second canonical form. This transformation includes the following steps: 1) Compute the elements b_{ijk}'s and d_{ij}'s from the elements a_{ijk}'s and c_{ij}'s by use of the recursive formulas (11) and (12). 2) Compute the matrix T_2 of (8) and then calculate the new output matrix.

Finally if it is required, instead, that the pair (F', H') is in a canonical form, the algorithm described above can be still used, but this time the rows of the Hankel matrix $T(0, n-1)$ should be used to calculate the canonical form required.

4. STOCHASTIC REALIZATION

In this section the minimal realization algorithm of the last section and the generalized companion form given by Luo and Bullock[12] will be combined to solve an realization problem for stochastic linear constant systems. This method yields substantial

savings in computation and leads to a formula which explicitly describes the redundancy in the system noise covariance.

Consider a stochastic linear constant system described by the difference equation

$$x(t+1) = Fx(t) + w(t)$$
$$y(t) = Hx(t) \tag{16}$$

where $x(t)$ is a stationary random variable, $w(t)$ is a Gaussian white noise with zero mean, and $y(t)$ is a stationary random variable and has full rank, i.e., $Ey(t)\,y'(t)$ is positive definite. Since the system is stationary, the eigenvalues of F all lie inside the unit circle. Define

$$Q = Ew(t)\,w'(t), \qquad M = Ex(t)\,x'(t)$$
$$C_i = Ey(t)\,y'(t+i) \qquad i = 0, 1, 2, \ldots$$

It is easily shown that the covariance function C_i and the covariance M satisfy the following equations

$$C_i = HF^i MH' \qquad i = 0, 1, 2, \ldots . \tag{17}$$

$$M = FMF' + Q. \tag{18}$$

The stochastic realization problem is this: Given the infinite sequence of $p \times p$ matrices $C_0, C_1, \ldots$, find a triple (F, H, Q) such that the equations (17) and (18) hold. The algorithm which will be given to identify the triple (F, H, Q) consists of two major parts. First, the realization technique of the last section is employed to obtain a minimal realization (F, G, H) such that the following equation is satisfied

$$C_i = HF^i G \qquad i = 0, 1, 2, \ldots \tag{19}$$

In computing (F, G, H), the pair (F′, H′) is specified to be in the second canonical form. Comparing (17) and (19), we have

$$G = MH' \tag{20}$$

The next step is to compute M using (20) and then to compute Q using (18). Since H is in general not nonsingular, not all entries

in M can be obtained by solving (20). It follows that it is impossible to completely identify Q by (18). To what extent can Q be identified? In the following the nonuniqueness in the identification of Q is described.

A suitable approach for the identification of Q is to use the generalized companion form[12]. The generalized companion form is a modification of Luenberger's second canonical form. If (F′, H′) is in Luenberger's second form, then by simply adding null state variables and rearranging all the state variables, the pair (F, H) can be transformed to the form

$$\hat{F} = \begin{bmatrix} 0 & 0 \dots & B_1 \\ I & 0 \dots & B_2 \\ \vdots & & \\ 0 & 0 \dots & I\, B_\nu \end{bmatrix} \qquad (21)$$

$$\hat{H} = [0 \quad 0 \dots D]$$

where I is the $p \times p$ identity matrix, B_i is a $p \times p$ matrix with entries b_{ijk}'s, D is a $p \times p$ lower triangular matrix with entries d_{ij}'s in the lower triangle, and ν is the observability index of the pair (F, H).

From now on, the pair (F, H) will be assumed in the generalized companion form and every matrix is partitioned into $p \times p$ blocks. For example:

$$G = \begin{bmatrix} G_1 \\ G_2 \\ \vdots \\ G_\nu \end{bmatrix} \quad Q = \begin{bmatrix} Q_{11} & Q_{12} \dots & Q_{1\nu} \\ Q_{21} & Q_{22} \dots & Q_{2\nu} \\ \vdots & & \\ Q_{\nu 1} & Q_{\nu 2} \dots & Q_{\nu\nu} \end{bmatrix}$$

where G_i and Q_{ii} are $p \times p$ matrices. Notice that the rows and the columns of G and Q which correspond to the added null state variables are zero.

With respect to the new equivalent system, MH′ is equal to the last p columns of M multiplied by D′, i.e.

$$MH' = \begin{bmatrix} M_{1\nu} D' \\ M_{2\nu} D' \\ \vdots \\ M_{\nu\nu} D' \end{bmatrix} \tag{22}$$

In view of (20) and (22), we note that the last p columns of M can be identified from the output covariance function C_i, while the rest can not.

Let $M_{ij} = 0$ if either i or j is zero. Then (18) can be simplified to

$$M_{ij} = M_{(i-1)(j-1)} + Q_{ij} + B_i M'_{(j-1)\nu} + M_{(i-1)\nu} B'_j + B_i M_{\nu\nu} B'_j \qquad i, j = 1, \ldots, \nu .$$

By simple substitutions the entries of the last p columns of M can be expressed in terms of themselves as

$$M_{i\nu} = \sum_{j=1}^{i} Q_{(i+1-j)(\nu+1-j)} + \sum_{j=1}^{i} \{B_{i+1-j} M'_{(\nu-j)\nu} + M_{(i-j)\nu} B'_{\nu+1-j} + B_{i+1-j} M_{\nu\nu} B'_{\nu+1-j}\} \qquad i = 1, \ldots, \nu \tag{23}$$

Since $M_{\nu\nu}$ is symmetric, M has $np-p(p-1)/2$ distinct elements in the last p columns. Thus there are $np-p(p-1)/2$ independent equations in (23). Rearranging the terms in (23) yields

$$\sum_{j=1}^{i} Q_{(i+1-j)(\nu+1-j)} = M_{i\nu} - \sum_{j=1}^{i} \{B_{i+1-j} M'_{(\nu-j)\nu} + M_{(i-j)\nu} B'_{\nu+1-j} + B_{i+1-j} M_{\nu\nu} B'_{\nu+1-j}\} \qquad i = 1, \ldots, \nu \tag{24}$$

Since every term on the right-hand side of (24) is known, the block diagonal sums of Q on the left-hand side can be determined. It is stressed here that these block diagonal sums of Q are the only information about Q that can be obtained from the output covariance function C_i. In other words, two different Q's may lead to the same output covariance function C_i if they have equal block diagonal sums.

5. CONCLUSION

In this paper the algorithm for minimal realization in canonical forms and the solution of the covariance equations in the generalized companion form have been combined to solve an realization problem for stochastic linear constant systems. This method involves solving only simple algebraic equations and leads to a formula which explicitly describes the redundancy in the system noise covariance.

REFERENCES

(1) Mehra, R.K., "On-line identification of linear dynamic systems with applications to Kalman filtering," *IEEE Trans. Automat. Contr.*, vol. AC-16, pp. 12-21, Feb. 1971.

(2) Box, E.E.P. and G.M. Jenkins, *Statistical Models for Forecasting and Control.* San Francisco, Calif, *Holden-Day*, 1970.

(3) Wong, K.Y. and E. Polak, "Identification of linear discrete time systems using the instrumental variable method," *IEEE Trans. Automat. Contr.*, vol. AC-12, pp. 707-718, Dec. 1967.

(4) Carew, B. and P.R. Belanger, "Identification of optimum filter steady-state gain for systems with unknown noise covariances," *IEEE Trans. Automat. Contr.*, vol. AC-18, pp. 582-587, Dec. 1973.

(5) Mayne, D.Q., "A canonical model for identification of multivariable linear systems," *IEEE Trans. Automat. Contr.* vol. AC-17, pp. 728-729, Oct. 1972.

(6) Caines, P.E., "Unique state variable models with application to the identification of linear systems," *Int. J. Contr.*, vol. 16, pp. 939-44, 1972.

(7) Denham, M.J., "Canonical forms for the identification of multivariable linear systems," *IEEE Trans. Automat. Contr.*, vol. AC-19, pp. 646-656, Dec. 1974.

(8) Dickinson, B.W., T. Kailath, and M. Morf, "Canonical matrix fraction and state space descriptions for deterministic and stochastic linear systems," *IEEE Trans. Automat. Contr.*, vol. AC-19, pp. 656-667, Dec. 1974.

(9) Tse, E. and H. Weinert, "Structure determination and parameter identification for multivariable stochastic linear systems," *IEEE Trans. Automat. Contr.*, vol. AC-20, pp. 603-613, Oct. 1975.

(10) Brotherton, T.W. and P.E. Caines, "ARMA system identification via the Cholesky least squares method," *IEEE Trans. Automat. Contr.*, vol. AC-23, pp. 698-702, August 1978.

(11) Suen, L.C. and R. Liu, "Determination of the structure of multivariable stochastic linear systems," *IEEE Trans. Automat. Contr.*, vol. AC-23, pp. 458-464, June 1978.

(12) Luo, Z. and T.E. Bullock, "Discrete Kalman filtering using a generalized companion form," *IEEE Trans. Automat. Contr.*, vol. AC-20, pp. 227-230, Apr. 1975.

(13) Luenberger, D. G., "Canonical forms for linear multivariable systems," *IEEE Trans. Automat. Contr.*, vol. AC-12, pp. 290-293, June 1967.
(14) Popov, V. M., "Invariant description of linear time-invariant controllable systems," *SIAM J. Contr.*, vol. 10, pp. 252-264, May 1972.
(15) Kalman, R. E., "Kronecker invariants and feedback," in *Proc. NRL Math. Res. Center Conf.* Ordinary Differential Equations, June 1971.
(16) Rosenbrock, H. H., *State Space and Multivariable Theory*. New York: Wiley, 1970.
(17) Luo, Z., "Transformations between canonical forms for multivariable linear constant systems," *IEEE Trans. Automat. Contr.*, vol. AC-22, pp. 252-256, April 1977.
(18) Chan and Wang, "A basis for the controllable canonical form of linear time-invariant multiinput systems," *IEEE Trans. Automat. Contr.*, vol. AC-23, pp. 742-745, August 1978.
(19) Kalman, R. E., P. L. Falb, and M. A. Arbib, *Topics in Mathematical System Theory*. New York: McGraw-Hill, 1969.
(20) Kalman, R. E., "Mathematical description of linear dynamical systems," *SIAM J. Contr.*, vol. 1, pp. 152-192, 1963.
(21) Ho, B. L. and R. E. Kalman, "Effective construction of linear state variable models from input/output functions," *Regelungstechnik*, vol. 14, pp. 545-548, Jan. 1966.
(22) Ackermann, J. E. and R. S. Bucy, "Canonical minimal realization of a matrix of impulse response sequences," *Inform. Contr.*, vol. 19, pp. 224-231, Oct. 1971.
(23) Silverman, L. M., "Realization of linear dynamical system," *IEEE Trans. Automat. Contr.*, vol. AC-16, pp. 554-567, Dec. 1971.
(24) Rissanen, J., "Recursive identification of linear systems," *SIAM J. Contr.*, vol. 9, pp. 420-430, Aug. 1971.
(25) Roman, J. R. and T. E. Bullock, "Minimal partial realizations in a canonical form," *IEEE Trans. Automat. Contr.*, vol. AC-20, pp. 529-533, Aug. 1975.

DETERMINATION OF THE SPHERICALLY SYMMETRIC COMPONENTS OF POTASSIUM ION-SMALL MOLECULE POTENTIALS

FRANK E. BUDENHOLZER, SVD

ABSTRACT

Incomplete total cross sections have been measured for K^+ scattered by N_2, CO, CO_2, CH_4, C_2H_4, C_2H_6, CF_4 and SF_6 in the range $E\theta_R = 2$–100 eV deg. Here E is the energy of the K^+ beam and θ_R the apparatus resolution angle. The data has been analysed to obtain estimates of the spherically symmetric component of the ion-molecule potential in the region of the potential well. Detailed consideration has been given to the problem of inverting the data in such a way as to take proper consideration of the anisotropies present in these systems.

INTRODUCTION

The interaction of atomic ions and molecules is such that we would expect the formation of "ion-cluster" molecules, $M^+ - X$, where M is an atomic ion and X the neutral ligand. Such ion clusters have, in fact, been observed (most notably using mass spectrometer techniques) and, as expected, they are formed via a three body process,[7]

$$M^+ + X + X \rightarrow M^+ - X + X \qquad (1)$$

These clusters have a certain intrinsic interest as unique chemical species. This is, however, overshadowed by their important role in a broad range of chemical and biological systems. Eq. (1) represents the key steps in the solvation of ions in water or non-aqueous solvents.[8] Closely related to this is the important role that cluster ions play in the transport of ions across membranes from one solvent environment to another.[9] Finally the formation of cluster ions has been found to be an important process in the earth's ionosphere.[10]

Accurate ion-molecule potentials, particularly in the region of

the potential well, are of critical importance if we are to understand the nature of the bonding in these ion clusters. Among the various ion-molecule potentials that could be studied those of the alkali metal ions and small symmetric molecules are particularly interesting, for these systems are amenable to both experimental and theoretical analysis.

The interaction energy between an atomic ion and an atom or linear molecule can be described by the potential function $V(R, \psi)$, where R is the distance between the ion and the molecular center of mass and ψ is the angle between the molecular axis and the vector directed along R. In order to understand the source of these interactions, the potential is often expressed as a sum of terms where each term describes a particular aspect or asymptotic form of the true potential.

Short range forces are those that determine the interaction energy at internuclear distances where significant charge cloud overlap can occur. These forces are repulsive and can often be adequately described by a simple exponential term:

$$V_{rep}(R) = ae^{-\xi R}. \qquad (2)$$

Such a form completely neglects short range anisotropies. However these anisotropic terms are expected to be small and our results and those of other workers support this conclusion. If we are concerned only with moderate and low energies, a simple inverse power potential of the form

$$V_{rep}(R) = C_N / R^N \qquad (3)$$

is satisfactory. This form is often mathematically more convenient and proved adequate for our work.

Long range forces are primarily electrical in origin. They can be conveniently considered under the headings, electrostatic forces, induction or polarization forces and dispersion forces.

Electrostatic forces involve the interaction between the atomic ion (considered as a point charge) and the permanent moments of

the molecule. For an ion-linear molecule potential, the most important electrostatic terms arise from the ion-dipole and ion-quadrupole interactions.[1]

$$V_{el}(R, \psi) = \frac{-eD}{R^2} P_1(\cos\psi) + \frac{e\vartheta_q}{R^3} P_2(\cos\psi) \qquad (4)$$

Here e is the electronic charge, D and ϑ_q are the dipole and quadrupole moments respectively, and $P_1(X)$ and $P_2(X)$ are the first and second Legendre polynomials. Terms involving moments of higher order have not been included.

The induction or polarization energy corresponds to the interaction of the ionic charge and the multipole moments induced in the molecule by the ion. For our purposes the most important terms are given by[1]

$$V_p(R, \psi) = -\frac{1}{2} \cdot \frac{e^2}{R^4} \{\alpha + 2\alpha\kappa P_2(\cos\psi)\} - \frac{e^2\alpha_q}{2R^6} . \qquad (5)$$

Here α is the average dipole polarizability and κ the anisotropy in the polarizability:

$$\alpha = \frac{1}{3}(\alpha_{\parallel} + 2\alpha_{\perp}) \qquad (6a)$$

$$\kappa = (\alpha_{\parallel} - \alpha_{\perp}) / (\alpha_{\parallel} + 2\alpha_{\perp}) . \qquad (6b)$$

The terms $\alpha_{\parallel}$ and $\alpha_{\perp}$ are defined as the dipole polarizabilities parallel and perpendicular to the molecular axis. Note that in using α it is important to include both the electronic and nuclear components to the polarizability.[3] The α_q of Eq. (5) is the field gradient quadrupole polarizability. Accurate values of α_q are not known for most small molecules. However Gislason and Rajan[4] have developed a semi-empirical method of predicting α_q from known values of α.

The dispersion energy is of quantum mechanical origin. It can, however, be visualized as an instantaneous dipole in one molecule inducing instantaneous multipoles in the opposite atom or molecule. For our purposes the only significant dispersion term is the so called induced dipole-induced dipole term:[1]

$$V_{disp}(R, \psi) = -\frac{C_{disp}}{R^6}\{1 + \kappa P_2(\cos\psi)\}. \quad (7)$$

C_{disp} can be calculated to sufficient accuracy for our work from known values of the dipole polarizability.[6]

The potential $V(R, \psi)$ can be expressed exactly as a sum over the complete set of Legendre polynomials:

$$V(R, \psi) = \sum_{l=0}^{\infty} V_l(R)\, P_l(\cos\psi). \quad (8)$$

Comparison with the various potential terms just described, indicates that the $l = 0$ to $l = 2$ terms are the most important. In what follows it will often be convenient to use the coefficients of Eq. (8) to indicate the various angularly dependent contributions to the total potential.

Using the various potential terms described above, relatively accurate potentials can be calculated for the long range ion-molecule interactions. A few calculations have also been carried out for ion-molecule systems in the region of the potential well. These include *ab initio* calculations, as for example those of Staemmler[2] for the Li^+–CO and Li^+–N_2 systems, and a recent "electron gas" calculation by Kim and Gordon.[5] However such calculations are far from routine and there is a need for empirically determined potentials in this critical region of the potential well.

Among the methods of determining ion-molecule and ion-atom potentials, molecular beam scattering experiments have been particularly fruitful. Both differential and incomplete total cross section measurements have been carried out.[11] Since detectors normally are unable to discriminate between various vibration-rotation states, the experimentally determined cross sections are usually sums over all final states.[12] This is the case for all of the work reported here.

The deconvolution of scattering data to obtain interatomic and intermolecular potentials has been the subject of much research.[13] With isotropic systems such as the alkali metal ion—rare gas systems, direct inversion of the data is in principle possible. However, the averaging involved in any beam experiment and the limited range

of the potential that any one experiment samples usually prohibit such a direct inversion. Rather a mathematical expression containing variable parameters is selected. "Experimental" cross sections are calculated from this potential and the parameters are then varied until a "best fit" potential is obtained.[14]

In the case of anisotropic systems the problem of inversion is considerably more complicated. If no external fields are present, we can begin with the assumption that all orientations of the scattering partners are equally probable. This implies that in calculating cross sections we must average over all molecular orientations.

In most theoretical calculations and inversion schemes a further assumption is made that the orientation of the molecule remains fixed during the time of the collision. If d defines the radius of significant interaction and v is the relative velocity, then this assumption is well justified when d/v is much smaller than the rotational period of the molecule. This is usually the case for the scattering of thermal atomic beams by diatomics and is clearly justified in the case of higher energy ion-small molecule systems such as those described in this report.

Initially it was usually assumed that for mildly anisotropic molecular systems, the orientation averaged scattering would be equivalent to scattering from a spherically averaged potential. In the case of rapid molecular rotation this is clearly a good approximation. However, even when the assumption of fixed orientation during the collision is made, the assumption is often justified. In an early calculation for the He–N_2 system Sinanoglu[15] compared cross sections calculated from a pre-averaged potential with orientation averaged cross sections. He found a difference of about 4%, comparable with the uncertainty in most beam experiments. A later calculation of Cross and Herschbach[16] as well as subsequent trajectory calculations[17] confirmed this conclusion.

However, when one wishes to consider the details of the scattering patterns, particularly in the area of the rainbow, such an assumption may lead to serious problems. For example, Cross[18] showed that glory undulations in energy dependent total cross

sections are quenched by molecular anisotropy. Budenholzer and Gislason[19] in a purely classical Monte-Carlo calculation of differential cross sections obtained results qualitatively similar to those of Buck, Gesterman and Pauly in a semi-classical calculation.[20] When mild P_1 and P_2 anisotropies are present the rainbow pattern is quenched and in the case of P_2 anisotropy a structure possibly indicating a second classical rainbow is observed.

A very recent paper compares accurate close coupling calculations with semi-classical orientation averaged cross sections and semi-classical cross sections using a spherically averaged potential. Both the close coupling results and the orientation averaged semi-classical results show a considerable damping of the oscillations found in the cross sections calculated using the pre-averaged potential.[21]

The damping of oscillations is seen very clearly in the work of Udseth, Giese and Gentry[22] who measured differential cross sections for the scattering of protons by Ar and various small diatomics. The rainbow pattern is quite clear for the H^+–Ar system, somewhat damped in the case of H^+–N_2($|\vartheta_q| = 1.5$), very weak for CO($|\vartheta_q| = 2.0$, D = 0.112) and completely absent from HCl(D = 1.1).

In the work that is reported here, we are attempting to obtain the maximum amount of potential information from incomplete total cross section data for the scattering of K^+ ions from various small molecules. Since our data is sensitive to the region of the potential well, we would expect the contribution from the anisotropy to be significant.

To describe the spherically symmetric contribution to the potential (V_0), we have used a simple inverse power potential of the form

$$V_0(R) = \frac{C_N}{R^N} - \frac{C_4}{R^4} - \frac{C_6}{R^6} . \qquad (9)$$

The R^{-4} term corresponds to the ion-induced dipole term of Eq. (5) and C_4 is set to its asymptotic value to guarantee proper behavior of the potential at large R. The parameters N, C_N, and C_6 are

then allowed to vary until an optimal fit to the data has been obtained.

In the literature, the spherically symmetric potentials are most often reported in terms of the position of zero potential energy (R_0), the position of the potential minimum (R_m), and the depth of the potential well (ε). These parameters are, of course, uniquely determined by Eq. (9).

In what follows a method to determine this spherically symmetric component to the ion-molecule potential is developed and the results of our analysis for various K^+- small molecule systems are presented.

EXPERIMENTAL PROCEDURE

The details of the experimental procedure have been described elsewhere.[23,24] Figure 1 shows schematically the principle components of the apparatus. Briefly, the incomplete total cross section Q is determined by measuring the attenuation of a K^+ beam, of LAB energy E, by a gas in a scattering chamber of length l at a pressure p. The K^+ beam is produced by surface ionization,

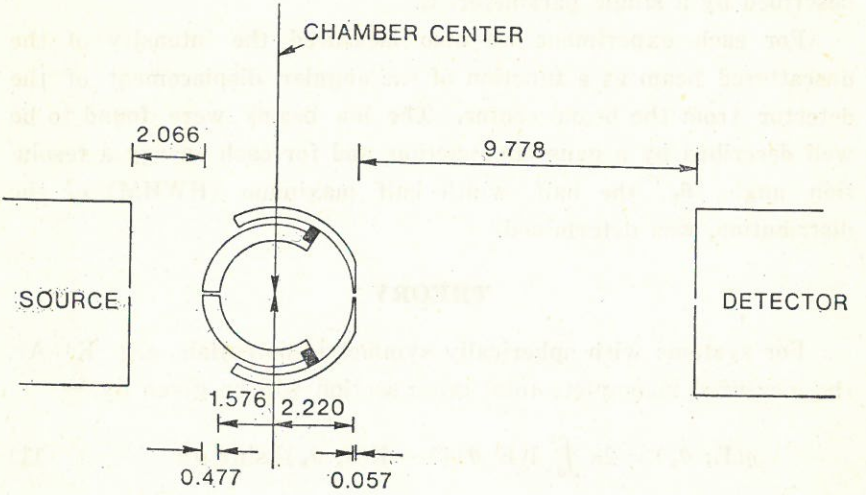

Fig. 1. Scale drawing of the principle components of the scattering chamber.

extracted, and focused through the scattering chamber onto a Faraday cup detector. The pressure of the scattering gas is measured with a capacitance manometer. All the collimating holes are circular, so the beam has cylindrical symmetry.

The cross section at each energy was determined from a modified Beer's law expression:

$$(nl)^{-1} \ln(I/I_0) = -Q + anlQ^2 . \tag{10}$$

Here I_0 is the K^+ intensity with no gas in the chamber; and n is the number density of the gas which is directly related to the pressure by the ideal gas law. The final term in Eq. (10) accounts for multiple scattering of K^+ ions in the scattering chamber. Both Q and a are determined by a least squares fit to Eq. (10). Typically seven data points were used in the fit. The uncertainty ΔQ in each cross section was estimated from the quality of the fit. Values of ΔQ averaged 6% of Q with low energy experiments having larger uncertainties.

For each experiment the energy distribution of the ion beam was determined using a retarding field energy analyser located in front of the Faraday cup. The spread in beam energies was relatively low, allowing the energy of the beam to be adequately described by a single parameter, E.

For each experiment we also measured the intensity of the unscattered beam as a function of the angular displacement of the detector from the beam center. The ion beams were found to be well described by a gaussian function, and for each energy a resolution angle, θ_R, the half width half maximum (HWHM) of the distribution, was determined.

THEORY

For systems with spherically symmetric potentials, e.g. K^+–Ar, the measured incomplete total cross section will be given by,[25]

$$q(E;\ \theta_R) = 2\pi \int_0^{\pi} I(E,\ \theta)\,[1 - K(\theta;\ \theta_R)] \sin\theta\, d\theta \tag{11}$$

Here $I(E, \theta)$ is the differential cross section in laboratory (LAB)

coordinates and $K(\theta;\ \theta_R)$ is the resolution function of the apparatus. $K(\theta,\ \theta_R)$ is simply the fraction of the ion beam which hits the detector after being scattered through LAB angle θ. (In what follows E and θ will refer to LAB coordinates and E_{rel} and ϑ to center of mass, CM, coordinates.)

In an apparatus with cylindrical symmetry such as ours, this $K(\theta;\ \theta_R)$ corresponds to the angular distribution of the unscattered gas normalized to one at the maximum.[23] Thus,

$$K(\theta;\ \theta_R) = \exp\left[-(\ln 2)\,(\theta/\theta_R)^2\right]. \tag{12}$$

In words Eq. (11) indicates that the cross section q (which is calculated cross section, corresponding to an actual experimental cross section Q) is the integral of the differential cross section over those angles where the particles miss the detector and are therefore counted as scattered.

In order to determine the "best fit" potential, Eq. (11) must be transformed so that it is an explicit function of the potential. We begin by considering the conservation of flux relationship from elementary scattering theory,

$$2\pi\, I(E,\ \theta)\sin\theta\, d\theta = 2\pi\, b\, db. \tag{13}$$

Here $I(E,\ \theta)$ is the differential cross section as previously defined and b is the impact parameter (the distance of closest approach between the scattering partners in the *absence* of a force). If Eq. (13) is substituted into Eq. (11) and appropriate changes are made in the limits of integration, we obtain

$$q(E;\ \theta_R) = 2\pi \int_0^\infty b[1 - K(\theta;\ \theta_R)]\, db \tag{14}$$

where $K(\theta;\ \theta_R)$ must now be expressed as a function of the impact parameter b and the intermolecular potential V(R).

Smith[26] has derived an expression which allows us to express the CM scattering angle (the angle between the initial and final relative velocity vectors) as a function of the impact parameter and the relative kinetic energy, E_{rel}:

$$E_{rel}\,\vartheta = \tau(b) + (E_{rel})^{-1}\tau_1(b) + (E_{rel})^{-2}\tau_2(b) + \ldots \tag{15}$$

$\tau(b)$, $\tau_1(b)$, etc. can be computed from the potential V(R). For inverse power potentials there exists a simple closed form solution. Furthermore at the high energies and small angles considered in this report only the first term in the expansion need be retained.[23]

All of the experimentally measured quantities are in LAB coordinates. If we assume that the motion of the scattering gas is negligible in comparison to that of the ion beam[23] and make approximations consistent with high energies and small angles, then using the standard LAB to CM transformation,[27] we obtain

$$E_{rel} = ME / (M + m) \tag{16a}$$

$$\vartheta = (M + m)\,\theta / M \tag{16b}$$

Here M is the mass of the scattering particle and m the mass of the ion. If this result is combined with Eq. (15), we obtain our basic working equation,

$$E\theta = E_{rel}\,\vartheta = \tau(b)\,. \tag{17}$$

We will refer to the product $E\theta$ as the reduced deflection angle and to $\tau(b)$ as the (reduced) deflection function. Eq. (17) states in words that the product of the LAB energy and scattering angle is a unique function of the impact parameter. The importance of this relation lies in the fact that, for a given system, it allows us to analyse data taken at different energies and with different apparatus resolution angles in terms of a single deflection function.

Figure 2 shows a typical deflection function. For such a function $\tau(b)$ is positive at small b, goes to zero at b_g, the glory impact parameter, and reaches a minimum value of $-\tau_r$ at b_r, the rainbow impact parameter. The function then goes smoothly to zero as b goes to infinity. Since a molecular beam apparatus has no way to distinguish positive from negative deflections, each $\tau_0 = E\theta_0$ will correspond to one or three impact parameters: one if $E\theta_0$ is greater than τ_r and three if $E\theta_0$ is less that τ_r.

The calculation of the deflection angle is carried out in a space-fixed coordinate system with the z axis chosen parallel to the initial relative velocity and the y axis defined by the initial orbital angular

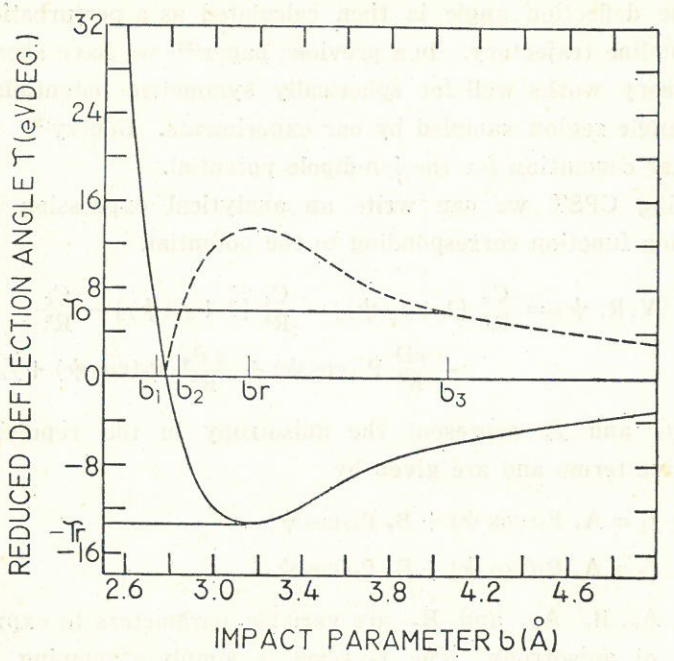

Fig. 2. The deflection function, $\tau(b)$, for the spherically symmetric K+-Ar system.

momentum. In the case of spherically symmetric potentials, scattering will take place entirely in the $x-z$ plane. However with the introduction of anisotropy, there is also an out-of-plane scattering component. The in-plane reduced deflection angle is given by

$$\tau_x = E_{rel}\,\vartheta_x \tag{18a}$$

where ϑ_x is the CM deflection angle in the $x-z$ plane. Similarly the out-of-plane component is given by

$$\tau_y = E_{rel}\,\vartheta_y\,. \tag{18b}$$

Simple geometric considerations indicate that, for small angles

$$(E_{rel}\,\vartheta)^2 = \tau^2 = \tau_x^2 + \tau_y^2\,. \tag{18c}$$

The deflection funcions, $\tau_x(b)$ and $\tau_y(b)$, are calculated using classical perturbation scattering theory (CPST).[28,29] It is assumed that the molecule does not rotate on the time scale of the collision

and the deflection angle is then calculated as a perturbation on a straight line trajectory. In a previous paper[23] we have shown that this theory works well for spherically symmetric potentials in the small angle region sampled by our experiments. Gentry[30] reached a similar conclusion for the ion-dipole potential.

Using CPST we can write an analytical expression for the deflection function corresponding to the potential,

$$V(R, \psi) = \frac{C_N}{R^N}[1+f_1(\psi)] - \frac{C_4}{R^4}[1+f_2(\psi)] - \frac{C_6}{R^6} - \frac{eD}{R^2}P_1(\cos\psi) + \frac{e\vartheta_q}{R^3}P_2(\cos\psi) + f_3 . \quad (19)$$

Here f_1 and f_2 represent the anisotropy in the repulsive and attractive terms and are given by

$$f_1 = A_r P_1(\cos\psi) + B_r P_2(\cos\psi) \quad (20a)$$

$$f_2 = A_a P_1(\cos\psi) + B_a P_2(\cos\psi) , \quad (20b)$$

where A_r, B_r, A_a, and B_a are variable parameters to express the degree of anisotropy. The f_3 term is simply a damping term to remove the dipole and quadrupole contributions at small R. The other variables have all been previously defined (see Eq. (9)). The precise form of the damping term and the corresponding deflection function are given in the appendix.

If the angles β and γ are used to define the orientation of the molecule with reference to the z axis of the space fixed coordinate system, then Eq. (14) can be extended to explicitly include the averaging over the various orientations of the molecule:

$$q(\tau_R) = \frac{1}{2}\int_0^\infty db \int_0^\pi d\beta \int_0^{2\pi} d\gamma\, b \sin\beta \{1 - \exp[-(\ln 2)(\tau(b, \gamma, \beta)/\tau_R)^2]\} \quad (21)$$

Here τ_R is the resolution angle of the apparatus, $\tau_R = E\theta_R$, and $\tau(b, \gamma, \beta)$ is given by Eqs. (A3) and (A5).

The integral of Eq. (21) can easily be solved on a computer using Gaussian quadrature routines. With this result we are in a position to calculate cross sections for comparison with experimental data.

However, before presenting our results, a few words should be said about the classical nature of our calculations. It is well known that at high energies, far outside the rainbow region, quantal effects can be ignored. That this should be possible in the rainbow region is somewhat surprising. A consideration of Eq. (11), however, gives a qualitative indication of why this is possible. Eq. (11) indicates that the calculated cross section represents both an integration over the differential cross section and an averaging over the resolution function. In a previous paper[28] we present a series of calculations for the K^+–Ar system which indicate that after this averaging has been carried out, the quantal and classical cross sections never differ by more than about 1%.

DATA ANALYSIS AND RESULTS

To gain a better understanding of the effect of anisotropies on incomplete total cross sections, trial data was first generated using Eq. (21) and the potential of Eq. (19). In these trial calculations $N = 8$, $C_8 = 230.2$ eV Å^8, $C_4 = 11.8$ eV Å^4 and C_6 was set to zero. These terms, chosen to approximate the K^+–Ar potential, were kept constant and cross sections were calculated using various values for the dipole, quadrupole and anisotropy coefficients (A_r, B_r, A_a, B_a).

Figures 3 and 4 display some of the trial data as a function of the resolution angle $E\theta_R$. In both figures cross sections for the spherically symmetric potential are indicated by solid lines. Dashed lines indicate cross sections calculated with anisotropy coefficients of 1.0 in Fig. 3 and 0.5 in Fig. 4; while the dash-dot lines indicate all four coefficients to be zero.

The upper curve of Fig. 3 demonstrates that with a dipole of 1.0 Debye (for HCl, D = 1.11 Debye), the ion-dipole term of the potential dominates the cross section at low energies and at moderate energies well beyond the region of the rainbow angle. However, at high energies ($\tau_R > 400$ eV deg.), the curves for the dipole moment of 1.0 D and the spherically symmetric case merge together smoothly. At this point the repulsive term in R^{-8} is completely dominating.

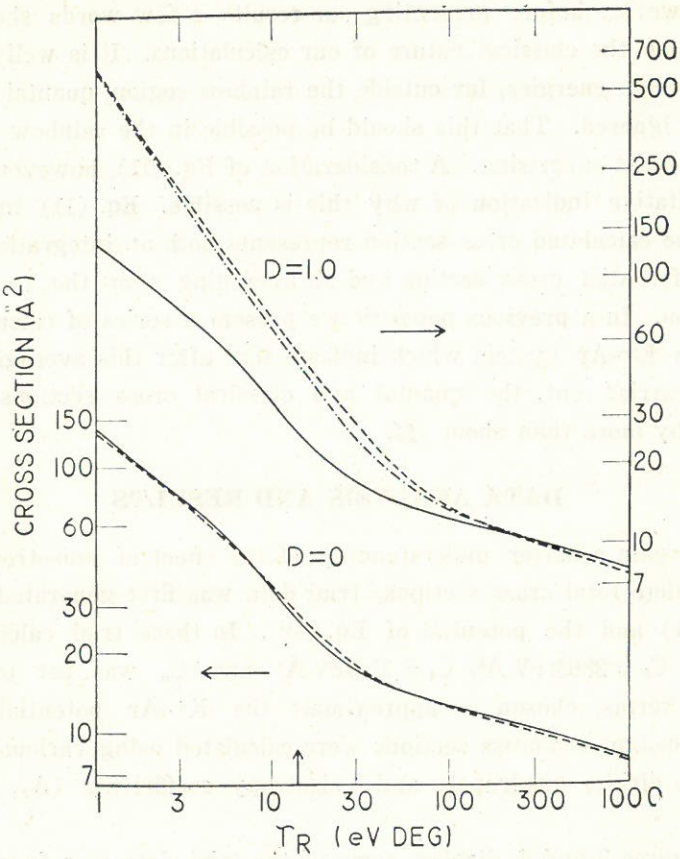

Fig. 3. Incomplete total cross sections for ion-dipole scattering.

It is also important to note that the effect of the anisotropy coefficients is magnified, particularly around the rainbow angle, when a strong dipole is present. Inspection of Eq. (21) indicates that the magnitude of the cross section is a function of τ^2. We therefore presume that this enhancement is due to the cross products of the various P_l terms. In contrast to this the lower curve of Fig. 3 indicates the relatively mild effect of the anisotropy coefficients when no dipole is present.

In Fig. 4 similar but less dramatic effects are seen when a large quadrupole is present. For a moderate quadrupole of 2.0 Quad

(10^{-26} esu cm^2) (the quadrupole moment of CO is 2.0 Quad), the quadrupole dominates at low energies only, though its effects are present well past the rainbow region.

This trial data was first fit to a potential of the form of Eq. (9). The spherically symmetric potential for each set of trial data is the same, and our goal was to see if a naive analysis of the data, completely ignoring anisotropic potential terms, would reproduce the spherically symmetric potential. We found that if no permanent dipole or quadrupole terms are present, moderate anisotropies could be neglected. Thus, for example, when we determined the best fit spherically symmetric potential for trial cross sections with the anisotropy coefficients all set to unity and the permanent molecular moments all set to zero, the rainbow angle, τ_r, and the well depth, ϵ, (the most sensitive of the potential parameters) differed from the

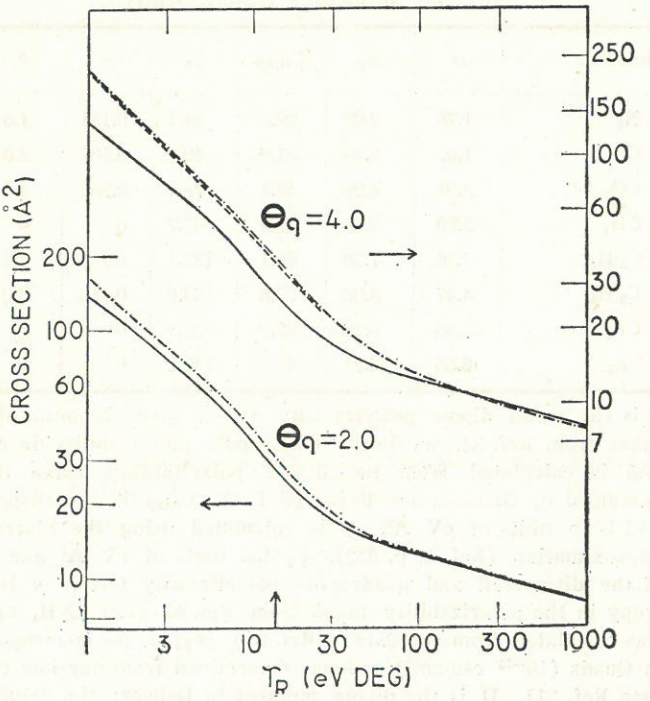

Fig. 4. Incomplete total cross sections for ion-quadrupole scattering.

exact spherically symmetric values by only about 7%. This should be compared with an average experimental error of about 8%.

However, we also found that even small dipole and quadrupole terms could not be neglected. Thus when we fit trial cross sections calculated with a quadrupole of only 2.0 Quads, and the anisotropy coefficients all zero, the resulting rainbow angle and well depth differed from the spherically symmetric value by more than 35%.

On the basis of these results, and on inspection of the literature values for the anisotropies in the polarizability of the molecules under study (see Table 1), we concluded that the ion-molecule potentials could be adequately described by potential functions which included only the anisotropy arising from the permanent dipole and quadrupole, and that all other anisotropies could be safely neglected.

Table 1. Summary of the Long Range Potential Parameters for the Molecules Under Study[a]

Molecule	α	α_q	C_{disp}	C_6	κ	$\lvert\theta_q\rvert$	D
N_2	1.76	2.02	29.6	44.1	0.131	1.5	0
CO	1.97	2.39	31.9	49.1	0.167	2.0	0.112
CO_2	2.91	4.26	47.4	78.1	0.264	4.4	0
CH_4	2.59	3.58	41.9	67.7	0	0	0
C_2H_4	4.26	7.50	68.1	122.1	0.158	3.2	0
C_2H_6	4.47	8.06	75.6	133.6	0.113	3.0	0
CF_4	3.86	6.48	47.2	93.9	0	0	0
SF_6	6.55	14.21	46.9	149.2	0	0	0

[a] α is the mean dipole polarizability and is given in units of Å^3. It is taken from Ref. 34. α_q is the quadrupole polarizability in units of Å^5 and is calculated from the dipole polarizability using the method described by Gislason and Rajan (Ref. 4). C_{disp} is the dispersion term and is in units of eV Å^6. It is calculated using the Slater-Kirkwood approximation (Ref. 6, p. 252). C_6 has units of eV Å^6 and is the sum of the dispersion and quadrupole polarizability terms. κ is the anisotropy in the polarizability taken from Ref. 6. (For C_2H_4 and C_2H_6 κ was calculated from the data of Ref. 34) $|\vartheta_q|$ is the quadrupole moment in Quads (10^{-26} esu-cm^2) and was determined from our low energy data (see Ref. 31). D is the dipole moment in Debyes; the values are from Ref. 6.

Thus our experimental cross sections were analysed using a potential of the form of Eq. (19) with $f_1 = f_2 = 0$. Values for $|\vartheta_q|$ were taken from a previous analysis of our low energy data,[31] values of D and C_4 were found in the literature. The parameters N, C_N, and C_6 were allowed to vary until the best fit potential had been obtained.

The standard procedure for determining the best fit potential is to begin with a set of estimated values for the variable parameters, calculate the cross section for each data point, $q(\tau_R)_i$, and then compare these results with the actual experimental results, Q_i. The quality of the fit is measured by the parameter χ,

$$\chi^2 = \frac{1}{N} \sum_{i=1}^{N} [Q_i - q(\tau_R)_i]^2 / \Delta Q_i^2 \tag{22}$$

where N is the number of data points for a particular ion-molecule system (in our case 36 for each gas) and ΔQ is the experimental uncertainty. The other variables have all been previously defined. One or more of the fitting parameters are then systematically varied and for each change a new set of $q(\tau_R)_i$ are calculated and χ is computed. This procedure is continued until χ has been minimized.

In principle the complete integration of Eq. (21) over both the impact parameter and the orientation angles could be carried out for each set of trial variables. However this proved to be prohibitively expensive, and a more economical procedure was developed.

Using the initial estimated values for C_N, N, and C_6 and the literature values for D, ϑ_q, and C_4, the complete integral of Eq. (21), $q^*(\tau_R)_i$, is determined for each data point. A second cross section, $q^+(\tau_R)_i$, is then calculated using only the spherically symmetric part of the potential. Using these a "reduced" experimental cross section, $Q_i^{(r)}$, is then calculated from the experimental cross section Q_i.

$$Q_i^{(r)} = Q_i - q^*(\tau_R)_i + q^+(\tau_R)_i \tag{23}$$

This reduced cross section is simply the experimental cross section with the dipole and quadrupole contributions removed.

These reduced cross sections are then fit to the best spherically

symmetric 4 – 6 – N potential (Eq. (9)). These best fit parameters are then used to recalculate q^* and q^+ and a new set of reduced cross sections is obtained. This second set of reduced cross sections is again fit to the best 4 – 6 – N potential. The process is continued until the optimal fit is obtained. In most of our work three iterations were carried out; the potential parameters were successively varied by increments of 5%, 5%, and 1%.

To determine the conditions under which this approach would be adequate to determine V_0, we first fit our trial data using this procedure. We found that when there was significant anisotropy

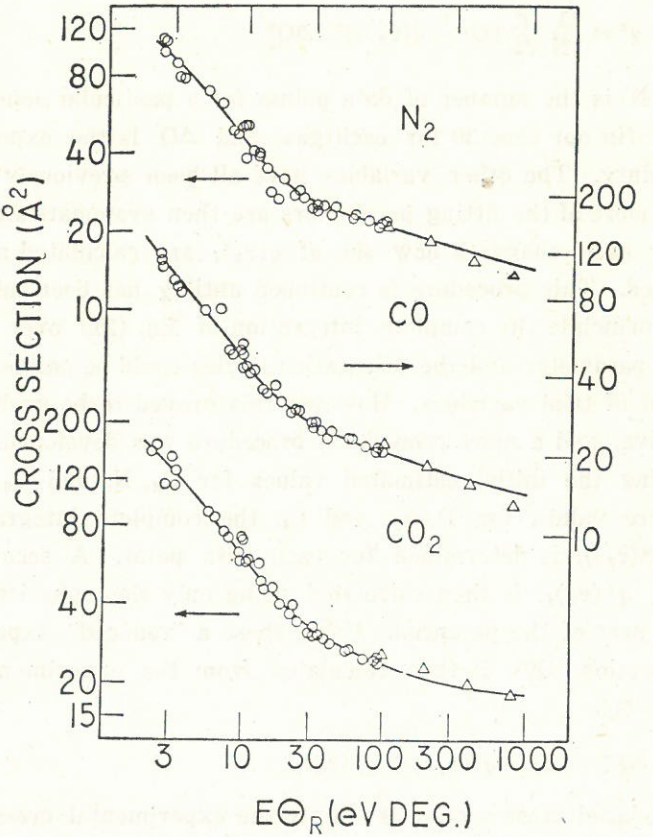

Fig. 5. Experimental (circles) and "best fit" total cross sections for the systems indicated.

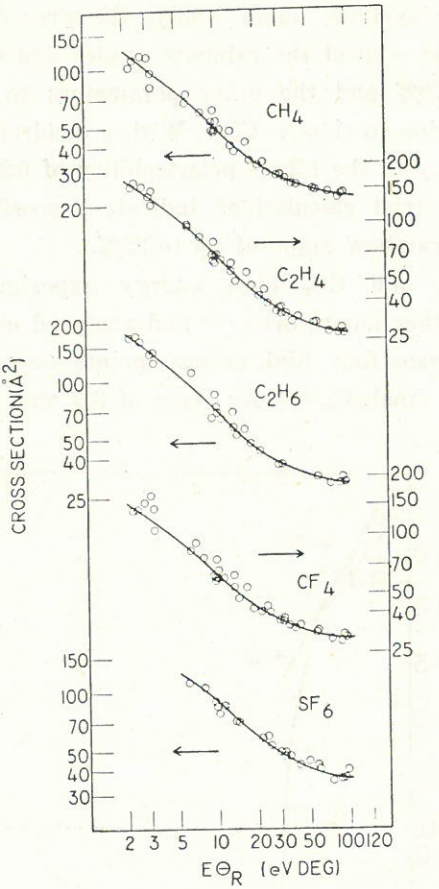

Fig. 6. Experimental (circles) and "best fit" total cross sections for systems indicated.

(A_r, B_r, A_a, $B_a \geq 0.5$) coupled with a moderate permanent dipole ($D \geq 1$) or a substantial quadrupole moment ($|\vartheta_q| \geq 4$), we were unable to obtain agreement in the well depth or rainbow angle to better than about 35%. This is the result of the coupling of the small anisotropies and the permanent multipole terms, as already discussed in the context of Figs. 3 and 4. This effect, resulting from the products of the various P_1 and P_2 terms is not removed by the procedure of Eq. (23).

However in the case of moderate anisotropies, such as those

occuring in the systems under study, the procedure is quite adequate. We would expect the rainbow angles and well depths to be good to within 10% and the other parameters to be even better. The only exception to this is CO_2. With a quadrupole of 4.4 Quads and an anisotropy in the dipole polarizability of 0.264 (equivalent to $B_a = 0.528$), the trial calculations indicate a possible error in the well depth and rainbow angle of up to 25%.

For N_2, CO, and CO_2 high energy experiments have been carried out in other laboratories,[32] and analysed using Eq. (2). For each of these gases four high energy points were synthesized and included in our analysis.[33] An error of 8% was assumed for the

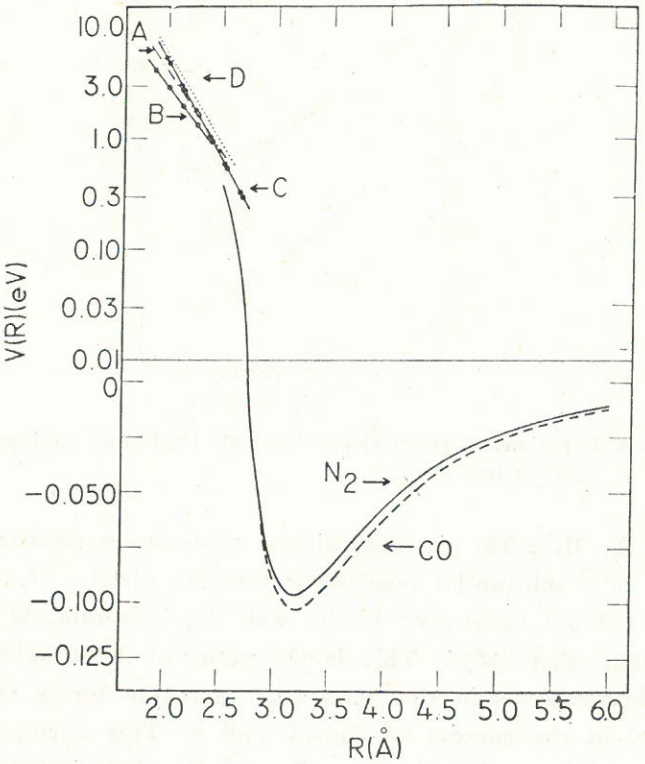

Fig. 7. Spherically symmetric component of the K+-CO and K+-N_2 potentials. Comparison with high energy results from other laboratories.

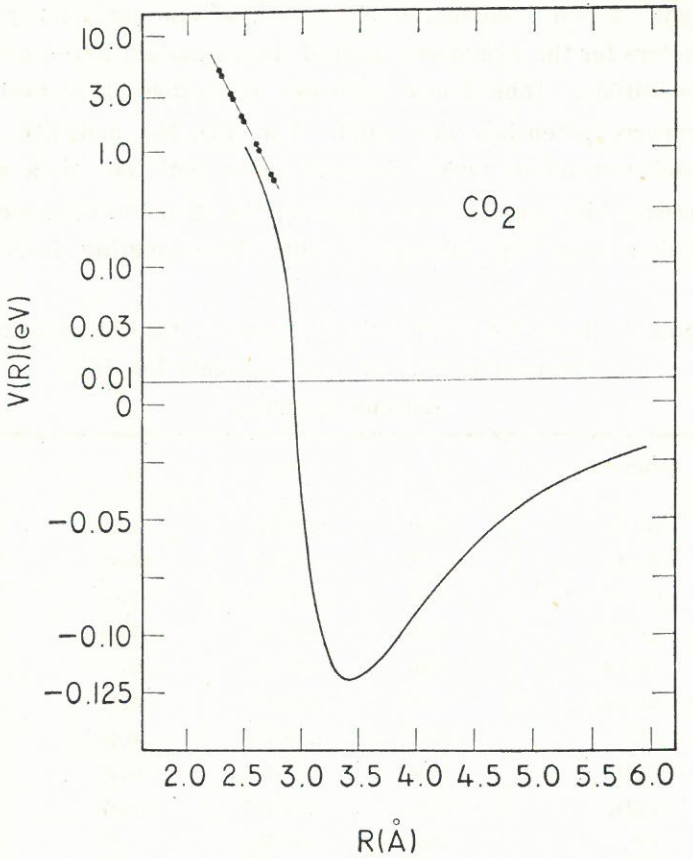

Fig. 8. Spherically symmetric portion of the K^+-CO_2 potential.

N_2 and CO data and 10% for the CO_2 data.

Figures 5 and 6 show the experimental data plotted as a function of the resolution angle $E\theta_R$. The synthesized high energy cross sections are also shown where appropriate. The solid lines represent the calculated cross sections, $q^*(\tau_R)_i$, which best fit the experimental data. Potential curves, V_0, for the potassium ion-CO, N_2, and CO_2 systems are shown in Figs. 7 and 8. These curves represent the potentials used in the calculation of the "best fit" cross sections of the previous figures. The high energy results from other laboratories are also included for comparison.

Tables 2 and 3 summarize the results of our analysis; potential parameters for the symmetric part of the potassium ion—small molecule potentials. Table 2 also indicates the range of R over which the various potentials are valid. For CO, N_2, and CO_2 the #1 potential parameters were obtained using both our data and the synthesized high energy cross sections; the #2 potential was obtained using data from our laboratory only. Extrapolating from earlier

Table 2. Best N-6-4 Potential Parameters for the Spherically Symmetric Part of the Potassium Ion-Small Molecule Potential[a]

Potential	N	C_N	C_6	C_4
N_2 #1	9.60	6.582 E3	73.24	12.67
N_2 #2	10.32	1.203 E4	56.89	12.67
CO #1	9.40	5.974 E3	79.35	14.18
CO #2	9.50	6.569 E3	77.89	14.18
CO_2 #1	8.80	7.535 E3	187.73	20.95
CO_2 #2	9.50	7.561 E3	187.73	20.95
CH_4	15.04	1.050 E6	0.42	18.65
C_2H_4	12.36	3.590 E5	66.37	30.67
C_2H_6	11.11	1.528 E5	119.47	32.18
CF_4	19.38	1.062 E9	7.41	27.79
SF_6	20.0[b]	1.489 E10	77.98	47.16

[a] The potential variables are defined by Eq. (9). The units of C_4, C_6, and C_N are respectively eV Å^4, eV Å^6, and eV Å^N. The #1 potential was determined using both our data and cross sections synthesized from the results of high energy experiments. The #2 potential was determined using only our data. The range of validity for these potentials (excluding high energy points from other sources) is:

N_2,	2.51-5.78 Å	CO	2.51-6.04 Å
CO_2,	2.68-7.03 Å	CH_4	2.53-6.39 Å
C_2H_4,	2.86-7.08 Å	C_2H_6	2.96-7.20 Å
CF_4,	3.03-7.00 Å	SF_6	3.26-5.82 Å

[b] In fitting the SF_6 data N took on unrealistically high values. For this reason N was not allowed to vary beyond 20. The value of χ obtained with this restriction was only slightly higher than that obtained when N was allowed to vary freely.

Table 3. Potential Parameters for the Spherically Symmetric Part of the Potassium Ion-Small Molecule Potential.[a]

Gas	ε	R_0	R_m	$(E\theta)_r$	χ
N_2 #1	0.096	2.76	3.20	9.64	0.81
N_2 #2	0.101	2.75	3.17	10.18	0.76
CO #1	0.103	2.76	3.21	10.27	0.75
CO #2	0.104	2.76	3.21	10.37	0.71
CO_2 #1	0.119	2.94	3.43	11.79	0.79
CO_2 #2	0.119	2.94	3.43	11.80	0.80
CH_4	0.161	2.69	3.04	16.88	0.70
C_2H_4	0.176	2.99	3.41	18.10	0.74
C_2H_6	0.146	3.14	3.61	14.88	0.90
CF_4	0.160	3.11	3.44	17.48	0.84
SF_6	0.218	3.37	3.72	24.16	0.67

[a] The well depth ε is given in eV. R_0 and R_m locate the potential zero and potential minimum in Å. The reduced rainbow angle $(E\theta)_r$ is given in eV deg. χ indicates the quality of fit and is defined by Eq. 22. The significance of the #1 and #2 potentials is indicated in Table 2 and in the text. Uncertainties are also given in the text.

work on K^+-rare gas potentials,[24] we estimate the following uncertainties: $\varepsilon \pm 40\%$; $R_0, \pm 6.5\%$; $R_m, \pm 10\%$; $(E\theta)_r, \pm 50\%$. It should be noted that these limits are wider than the errors in fitting the trial data using the method of Eq. (23), with the exception of those cases where a permanent dipole was involved.

DISCUSSION

A consideration of Figs. 3 and 4 indicates in a qualitative way the effects of various anisotropic terms on the total cross section; and also indicates the type and degree of information that can be obtained from total cross section measurements such as those carried out in our laboratory.

At high energies ($\tau \gg \tau_R$) the isotropic R^{-N} term clearly dominates the molecular scattering. Accurate calculation of short range forces is difficult, and little detailed experimental or theoretical information is available. However, within the limits of our

model calculations, our work indicates that at high energies small anisotropies will only mildly effect the total cross section. Hence we would agree with previous researchers that in this region a simple spherically symmetric function quite adequately represents the true potential.

At low energies, ion-molecule scattering is strongly dominated by the ion-dipole and ion-quadrupole terms. The fact that the remaining significant terms (ion induced dipole, ion induced quadrupole, and induced dipole-induced dipole) are well known, has allowed a determination of quadrupole moments from low energy scattering data.[31]

In the region of intermediate energy around the rainbow, the ion-molecule scattering is still strongly influenced by the presence of permanent dipole and quadrupole moments. There also appears to be some coupling between small P_1 and P_2 anisotropies with the permanent moments of the molecule. The stronger these anisotropic terms the more difficult it is to obtain detailed information on the symmetric part of the potential in this region. As would be expected, this result parallels the results found in differential cross section experiments and calculations. As was briefly indicated in the introduction, the presence of anisotropies tends to quench the rainbow oscillations, thereby limiting the amount of information available in such experiments.

When no permanent electrostatic moments are present, our results indicate that other small anisotropies—for example the anisotropy in the dipole polarizability,—are relatively insignificant in relation to the averaging and experimental uncertainty inherent in total cross section measurements. This would support the claim that in atom-molecule scattering a pre-averaged potential is usually adequate to interpret the scattering data. This, of course, also implies that it will be quite difficult to deconvolute such scattering data in such a way as to obtain detailed information on small potential anisotropies.

In the case of ion-molecule systems, ion-dipole and ion-quadrupole terms are usually present and these terms must be taken into

account if an accurate determination of the spherically symmetric potential is to be made. We believe that the procedure outlined above is quite satisfactory, given the normal degree of experimental uncertainty. We further believe that our estimates of error in the potential parameters are quite conservative and that the true potential parameters are well within these limits.

There are, at present, no other experimental or theoretical results with which to compare our work. However, the good agreement between potentials #1 and #2 for N_2, CO, and CO_2 in Tables 2 and 3 indicates the continuity of our results with the high energy scattering results from other laboratories.

Figure 7 and the results presented in the tables indicate near agreement between the N_2 and CO spherically symmetric potentials. This is as expected for the two ioselectronic species. The agreement between the C_6 coefficients of Table 2 and the accepted values listed in Table 1 seems somewhat less than satisfactory. However, the experimentally determined potential must be considered as a single flexible function. To expect one parameter of a three parameter fit to closely match its asymptotic value is unrealistic.

In summary, incomplete total cross sections have been measured for potassium ions scattered by various small molecules and the data inverted to obtain the spherically symmetric component of the ion-molecule potential. Detailed consideration has been given to the problem of inverting the data in such a way as to take proper consideration of the anisotropies present in these systems.

ACKNOWLEDGEMENTS

The work presented here was carried out under the direction of Eric A. Gislason at the University of Illinois, Chicago Circle. In the laboratory and preliminary data analysis, the author worked closely with Andrew Jorgensen. Their assistance is gratefully acknowledged.

APPENDIX

Calculation of the Deflection Function

Trial data were generated using a modification of the potential of Eq. (19).

$$V(R, \psi) = \frac{C_8}{R^8}\{1 + A_r P_1(\cos\psi) + B_r P_2(\cos\psi)\} - \frac{C_4}{R^4}\{1 + A_a P_1(\cos\psi) + B_a P_2(\cos\psi)\} + \left(\frac{C_7}{R^7} - \frac{eD}{R^2}\right) P_1(\cos\psi) + \left(\frac{S_7}{R^7} + \frac{e\vartheta_q}{R^3}\right) P_2(\cos\psi) \quad \text{(A1)}$$

The C_7 and S_7 terms damp the dipole and quadrupole at small R and are given by

$$C_7 = e D R_0^5 \quad \text{(A2a)}$$

$$S_7 = e\vartheta_q R_0^4. \quad \text{(A2b)}$$

The deflection function can be calculated using the formulas of Ref. (29).

$$\begin{aligned}\tau_x &= E\theta_x \\ &= \frac{C_8}{b^8}\left[\frac{35\pi}{32} + \frac{16}{5} A_r \sin\beta\cos\gamma - \frac{35\pi}{512} B_r(8 - 21\sin^2\beta\cos^2\gamma - 3\cos^2\beta)\right] \\ &\quad + \frac{C_4}{b^4}\left[-\frac{3\pi}{4} - 2A_a\sin\beta\cos\gamma + \frac{3\pi}{32} B_a(4 - 9\sin^2\beta\cos^2\gamma - 3\cos^2\beta)\right] \\ &\quad + \left[\frac{15\pi}{16}\frac{C_7}{b^7} - \frac{eD}{b^2}\right]\sin\beta\cos\gamma + \frac{e\vartheta_q}{b^3}\sin^2\beta\cos(2\gamma) \\ &\quad - \frac{S_7}{35\,b^7}[144\sin^2\beta\cos^2\gamma + 24\cos^2\beta - 56] \quad \text{(A3a)}\end{aligned}$$

$$\tau_y = E\,\theta_y$$
$$= \frac{C_8}{b^8}\left[-\frac{16}{35}A_r \sin\beta \sin\gamma - \frac{105\pi}{256}B_r \sin^2\beta \sin\gamma\cos\gamma\right]$$
$$+ \frac{C_4}{b^4}\left[\frac{2}{3}A_a \sin\beta\sin\gamma + \frac{9\pi}{16}B_a \sin^2\beta\sin\gamma\cos\gamma\right]$$
$$+ \left[\frac{-5\pi}{32}\frac{C_7}{b^7} + \frac{eD}{b^2}\right]\sin\beta\sin\gamma$$
$$- \frac{e\,\vartheta_q}{b^3}\sin^2\beta\sin(2\gamma)$$
$$+ \frac{48}{35}\frac{S_7}{b^7}[\sin^2\beta\sin\gamma\cos\gamma] \qquad \text{(A3b)}$$

$$\tau^2 = \tau_x^2 + \tau_y^2 \qquad \text{(A3c)}$$

The C_8 and C_6 coefficients are given in the body of the paper. Care must be taken that they are in the same angular units as the resolution angles, θ_R.

For the actual fitting of experimental data a more simple form of the potential was used

$$V(R,\psi) = \frac{C_N}{R^N} - \frac{C_4}{R^4} - \frac{C_6}{R^6} - \frac{eD}{R^2}P_1(\cos\psi)$$
$$+ \frac{e\,\vartheta_q}{R^3}P_2(\cos\psi)\,. \qquad \text{(A4)}$$

The deflection function is given by

$$\tau_x = C'_N/b^N - C'_4/b^4 - C'_6/b^6$$
$$+ \left\{\frac{-eD}{b^2}\sin\beta\cos\gamma\right.$$
$$\left. + \frac{e\,\vartheta_q}{b^3}\sin^2\beta\cos(2\gamma)\right\} f(b) \qquad \text{(A5a)}$$

$$\tau_y = \left\{\frac{eD}{b^2}\sin\beta\sin\gamma - \frac{e\,\vartheta_q}{b^3}\sin^2\beta\sin(2\gamma)\right\} f(b)\,. \qquad \text{(A5b)}$$

For the inverse power terms, the primed quantities are related to the potential terms as follows,

$$V(R) = C_N/R^N$$

$$\tau(b) = \frac{C'_N}{b^N} = \frac{C_N}{b^N}\sqrt{\pi}\,\frac{\Gamma(\frac{1}{2}N + \frac{1}{2})}{\Gamma(\frac{1}{2}N)} \qquad \text{(A6)}$$

where Γ indicates the gama function. The damping term is given by

$$f(b) = 0 \qquad 0 \leq b \leq b_g$$

$$f(b) = 1 - \exp\left[-(b/b_g)^2\right]. \qquad b_g \leq b \leq \infty$$

Here, b_g is the impact parameter where $\tau_x = 0$ for the spherically symmetric component of the deflection function.

DESCRIPTION OF FIGURES

Fig. 1. Scale drawing of the scattering chamber region showing the position of the ion source, the scattering cell, and the Faraday cup detector. The exit aperture of the source, the entrance and exit apertures of the scattering cell and the entrance aperture of the detector are each circular with 0.1 cm diameters. All dimensions are given in cm. The center of the vacuum chamber is located inside the scattering cell where the arrows meet. The effective length of the scattering cell, l, is 4.063 cm.

Fig. 2. The deflection function, $\tau(b)$, for the spherically symmetric K^+–Ar system. Here b_r is the rainbow impact parameter and τ_r the (reduced) rainbow angle. The dashed line represents the absolute value of the deflection function. The impact parameters b_1, b_2, and b_3 give scattering at the reduced deflection angle $\tau = \tau_0$. If we neglect the averaging over the deflection function, the corresponding incomplete total cross section would simply be $\sigma_0 = \pi(b_1^2 - b_2^2 + b_3^2)$.

Fig. 3. The incomplete total cross section, $q(\tau_R)$, plotted as a function of the resolution angle, τ_R. The cross sections were calculated using Eq. (21) and the potential of Eq. (19). The solid lines represent the spherically symmetric case. The dot-dash curve describes the cross section for D = 1.0 Debye and the anisotropy coefficients (A_r, B_r, A_a, B_a) equal to zero. In the dashed curves the anisotropy coefficients equal 1.0. In the upper curve this anisotropy is coupled with a dipole of 1.0 Debye; in the lower curve the dipole is zero.

The rainbow angle for the spherically symmetric case is 14.0 eV deg. and is marked with an arrow on the abscissa.

Fig. 4. Incomplete total cross sections calculated in the same manner as those in Fig. 3. In the upper dot-dash curve the quadrupole moment is 4.0 Quads with anisotropy coefficients of zero. For the lower dot-dash curve the quadrupole is 2.0 Quads and the anisotropy coefficients are also zero. The dashed curve represents cross sections calculated with a quadrupole moment of 4.0 Quads and anisotropy coefficients of 0.5. Note that in this case there is a slight diminishment of the cross sections. As in Fig. 3 the spherically symmetric case is represented by the solid line.

Fig. 5. Total cross sections in $Å^2$ plotted as a function of the resolution angle, $E\theta_R = \tau_R$, for the potassium ion-small molecule systems indicated. The experimental data are indicated by circles. The solid lines indicate the calculated cross sections, $q^*(\tau_R)$, that best fit our data. The triangles are the high energy cross sections synthesized from the potentials of other workers. (see Ref. 32 and 33.)

Fig. 6. Experimental and calculated cross sections, as in Fig. 5. Note that CH_4, SF_6, and CF_4 are spherically symmetric and therefore could be analysed using only the potential of Eq. (9).

Fig. 7. Potential curves describing the spherically symmetric part of the potential, V_0, for the K^+–N_2 and K^+–CO systems. The potentials are derived from our data plus the four synthesized high energy cross sections. For most of the region inside the potential minimum, the two curves are indistinguishable on the scale of the graph. Shown also are the high energy results of other workers: A, CO and N_2 results of Kita, Inouye, and Noda (Ref. 32(a)); B, N^2 and CO results of Van Dop, Boerboom, and Los (Ref. 32(b)); C, N_2 results of Amdur and co-workers (Ref. 32(c)); D CO results of Amdur and co-workers (Ref. 32(c)); notice the change in energy scale at 0.01 eV.

Fig. 8. Potential curve describing the spherically symmetric part of the potential for the K^+–CO_2 system. The notation is as in Fig. 7. The dash-dot curve is the potential derived by Amdur and co-workers (Ref. 32(c)) in high energy beam experiments.

REFERENCES

(1) Buckingham, A. D., *Advan. Chem. Phys.* **12**, 129 (1967).
(2) (a) Staemmler, V., *Chem. Phys.* **7**, 17 (1975). (b) Staemmler, V., *Chem. Phys.* **17**, 187 (1976).
(3) Gislason, E. A., F. E. Budenholzer and A. D. Jorgensen, *Chem. Phys. Lett.* **47**, 434 (1977).
(4) Gislason, E. A., and M. S. Rajan, *Chem. Phys. Lett.* **50**, 251 (1977).
(5) Kim, Y. S. and R. G. Gordan, *J. Chem. Phys.* **61**, 1 (1974).
(6) McDaniel, E. W. and E. A. Mason, *The Mobility and Diffusion of Ions in Gases*, Wiley-Interscience, New York (1973).
(7) Good, A., *Chem. Rev.* **75**, 561 (1975).
(8) Recent reviews include: (a) Durbin, J. and M. J. Henchman, *MTP International Review of Science*, ed. by J. C. Polanyi, Butterworths, London, (1972), Physical Chemistry Series 1, Vol. 9, p. 235. (b) Kebarle, P., in *Ion-Molecule Reactions*, ed. by J. L. Franklin, Plenum, New York, (1972), Vol. 1, Ch. 7. (c) Kebarle, P., *Mod. Asp. Electrochem.* **9**, 1 (1974).
(9) Hladky, S. B., L. G. M. Gordon and D. A. Haydon, *Ann. Rev. Phys. Chem.* **25**, 11 (1974).
(10) For recent reviews see: (a) Brown, T. L., *Chem. Rev.* **73**, 645 (1973). (b) Baggaley, W. J. and C. H. Cummack, *J. Atm. Terr. Phys.* **36**, 1759 (1974).
(11) See for a recent review see Cross, R. J., *Acc. Chem. Res.* **8**, 225 (1975). Also see references of Ref. 23.
(12) For a review of recent work that includes vibrational, rotational state selection, see Toennies, J. P., *Ann. Rev. Phys. Chem.* **27**, 225 (1976).
(13) Buck, U., *Rev. Mod. Phys.* **46**, 369 (1974).
(14) Budenholzer, F. E., E. A. Gislason and A. D. Jorgensen, *J. Chem. Phys.* **66**, 4832 (1977). In the above work a potential of the form of Eq. (9) is used. Other functional forms may be selected, see Siska, P. E., J. M. Schafer and Y. T. Lee, *J. Chem. Phys.* **55**, 5766 (1971).
(15) Sinanoglu, O., *J. Chem. Phys.* **30**, 850 (1959).
(16) Cross, R. J. and D. R. Herschbach, *J. Chem. Phys.* **43**, 3530 (1965).
(17) (a) LaBudde, R. A. and R. B. Bernstein, *J. Chem. Phys.* **55**, 5499 (1971). (b) Brown, N. J., *J. Chem. Phys.* **60**, 2958 (1974).
(18) Cross, R. J., *J. Chem. Phys.* **52**, 5703 (1970).
(19) Budenholzer, F. E. and E. A. Gislason, *J. Chem. Phys.* **68**, 4222 (1978).
(20) Buck, U., F. Gesterman and H. Pauly, *Chem. Phys. Lett.* **33**, 186 (1975).

(21) Goldflam, R., S. Green, D. J. Kouri and L. Monchick, *J. Chem. Phys.* **69**, 598 (1978).
(22) Udseth, H., C. F. Giese and W. R. Gentry, *J. Chem. Phys.* **60**, 3051 (1974).
(23) Budenholzer, F. E., E. A. Gislason and A. D. Jorgensen, *J. Chem. Phys.* **66**, 4832 (1977).
(24) Jorgensen, A. D., *Ph. D. Thesis*, University of Illinois at Chicago Circle, 1976.
(25) Gislason, E. A., *J. Chem. Phys.* **63**, 2828 (1975).
(26) Smith, F. T., R. P. Marchi and K. G. Dedrick, *Phys. Rev.* **150**, 79 (1966).
(27) Symon, K. R., *Mechanics*, Addison Wesley, Reading, Mass. (1971), p. 184.
(28) Cross, R. J., *J. Chem. Phys.* **46**, 609 (1967).
(29) Gislason, E. A. and J. G. Sachs, *Chem. Phys.* **25**, 155 (1977).
(30) Gentry, W. R., *J. Chem. Phys.* **60**, 2547 (1974).
(31) Budenholzer, F. E., E. A. Gislason, A. D. Jorgensen and J. G. Sachs, *Chem. Phys. Lett.* **47**, 429 (1977).
(32) (a) Kita, S., K. Noda, and H. Inouye, *Chem. Phys.* **7**, 156 (1975). (b) Van Dop, H., A. J. H. Boerboom and J. Los, *Physica* **61**, 626 (1972). (c) Amdur, I., J. E. Jordan, L. W. M. Fung, L. J. F. Hermans, S. E. Johnson and R. L. Hance, *J. Chem. Phys.* **59**, 5329 (1973).
(33) Budenholzer, F. E., *Ph. D. Thesis*, University of Illinois at Chicago Circle, 1977.
(34) Landolt-Bornstein, *Zahlenwerte und Funktionen*, Springer, Berlin (1971), Vol. 1, Part. 3, p. 514.

When any mortal (even the most odd)
Can justify the ways of man to God,
I'll think it strange that normal mortals can
Not justify the ways of God to man.

E. E. CUMMINGS

PYRROLYSIS AND PARTIAL OXIDATION OF BENZENE*

YUNG-NAN CHEN

ABSTRACT

The pyrrolysis of the mixture of benzene and steam, with or without oxygen over active carbon, aluminum oxide, silica gel, nickel aluminum alloy powder, platinum, vanadium pentoxide and copper has been studied.

In the absence of oxygen, biphenyl was isolated as the sole reaction product. In the presence of oxygen, biphenyl was similarly obtained with two exceptions: over vanadium pentoxide, the major product is p-benzoquinone and over copper, the major product is phenol.

INTRODUCTION

Phenol, an important industrial organic chemical, is obtained commercially from coal tar and by synthetic methods[1] like the sulfonation process, the Raschig process, the Dow toluene process and the Cumene process.

Most industrial synthetic methods for the production of phenol employ benzene as the starting material and require several expensive synthetic steps. A one-step change of benzene into phenol would lower the cost of commercial phenol. Recently, there have been many advances in this area of research.[2-6]

We have found that benzene may by transformed directly into phenol by the following methods:

(A) Hydrolysis of benzene in the presence of some catalyst, and under suitable conditions.

$$C_6H_6 + H_2O \xrightarrow[\Delta]{\text{cat.}} C_6H_5OH + H_2 \qquad (1)$$

(B) Hydrolysis of benzene in the presence of oxygen and some catalyst.

* This work was supported by The Chinese Petroleum Corporation.

(C) Partial oxidation of benzene in the presence of some catalyst.

$$2C_6H_6 + O_2 \xrightarrow[\Delta]{\text{cat.}} 2\,C_6H_5OH \qquad (2)$$

We chose catalysts that are commonly used in petroleum chemistry, including active carbon, aluminum oxide, nickel-aluminum alloy powder, silica gel, platinum, vanadium pentoxide and copper and studied their activity to catalize the methods (A), (B), (C).

EXPERIMENT

A. Instruments:

(1) Oven: Heraeus Macrocombustion Furnace Type KR 1700.
(2) Thermometer: Heraeus TAK Bestell Nr. 36512–060 Pt, Rh-Pt 0°–1600°C.
(3) Reactor: #304 stainless pipe 7/8″ O. D.
(4) Gas Chromatograph: Hewlett Packard 5700 with F. I. D.
(5) I. R. Spectrometer: Unicam Sp 1100.

B. Illustrative procedure:

100 ml of benzene was vaporized (0.35 ml/min) and mixed with steam ($C_6H_6 : H_2O = 1:1.5$). This mixture is passed into the preheated column at 360°C (200 mm in length) and then proceeds through the reactor at a temperature of 400°C (350 mm in length). The temperatures in each table are the temperatures of the reactor.

The products were collected through a water cooled condenser. The water layer was tested with 5% $FeCl_3$ solution and the organic layer was evaporated to free benzene. The residues were identified by I. R. spectrum, GLC analysis and physical data. The results are listed in the tables. (Tables 1 to 17).

DISCUSSION

In the absence of either catalyst or oxygen (nitrogen atmosphere) at temperatures ranging from 400° to 820°C no phenol is produced, but at temperatures ranging from 580° to 820° biphenyl is isolated (m. p. 69°–70°C). Its I. R. spectrum ν max cm^{-1}: 3080, 1605, 1580, 1490.

Table 1. Results of reactions without catalyst.
Carrier gas N_2 (60 ml/min).

Run No.	Temp. (°C)	Recovery C_6H_6 (ml)	$FeCl_3$ Test	Products
1	400	90	(−)	
2	460	90	(−)	
3	520	87	(−)	
4	580	85	(−)	[a]
5	640	82	(−)	0.1 g[b]
6	700	80	(−)	0.5 g[b]
7	760	75	(−)	1.2 g[b]
8	820	65	(−)	3.5 g[b] + C[c]
9[d]	760	75	(−)	1.1 g[b]
10[e]	760	75	(−)	1.0 g[b]
11[f]	760	70	(−)	1.0 g[b]

[a]: trace white solid.
[b]: biphenyl.
[c]: carbon.
[d]: $(C_6H_6) : (H_2O) = 1 : 0$
[e]: $(C_6H_6) : (H_2O) = 1 : 3$
[f]: $(C_6H_6) : (H_2O) = 1 : 5$

Table 2. Results of reactions without catalyst.
Carrier gas: air, (160 ml/min).

Run No.	Temp. (°C)	Recovery C_6H_6 (ml)	$FeCl_3$ Test	Products
1	400	90	(−)	
2	460	90	(−)	
3	520	89	(−)	[a]
4	580	85	(−)	0.1 g[b]
5	640	85	(−)	0.2 g[b]
6	760	75	(−)	3.5 g[b]
7	700	80	(−)	1.0 g[b]
8	760	70	(−)	3.1 g[b]
9	820	65	(−)	6.0 g[b]

[a]: trace white solid.
[b]: biphenyl.
[c]: carbon.

Table 3. Results of reactions using 40 grams of 1½ mm active carbon as catalyst.
Carrier gas: N_2 (160 ml/min).

Run No.	Temp. (°C)	Recovery C_6H_6 (ml)	$FeCl_3$ Test	Products
1	400	90	(−)	
2	460	90	(−)	
3	520	88	(−)	[a]
4	580	85	(−)	0.1 g[a]
5	640	82	(−)	0.5 g[b]
6	700	80	(−)	0.7 g[b]
7	760	75	(−)	1.5 g[b]
8	820	65	(−)	3.5 g[b] + C[c]

[a]: trace white solid.
[b]: biphenyl.
[c]: carbon.

Table 4. Results of reactions using 40 grams of 1½ mm active carbon as catalyst.
Carrier gas: air (160 ml/min).

Run No.	Temp. (°C)	Recovery C_6H_6 (ml)	$FeCl_3$ Test	Products
1	400	90	(−)	
2	460	90	(−)	[a]
3	520	85	(−)	[a]
4	580	85	(−)	0.1 g[b]
5	640	80	(−)	1.0 g[b]
6	700	75	(−)	2.2 g[b]
7	760	70	(−)	4.6 g[b]
8	820	60	(−)	6.2 g[b] + C[c]

[a]: trace white solid.
[b]: biphenyl.
[c]: carbon.

Table 5. Results of reactions using 5g of 500 mesh Al_2O_3 coating on 10g of pyrex glass wool as catalyst. Carrier gas: N_2 (160 ml/min).

Run No.	Temp. (°C)	Recovery C_6H_6 (ml)	$FeCl_3$ Test	Products
1	400	90	(−)	
2	460	90	(−)	
3	520	87	(−)	[a]
4	580	85	(−)	[a]
5	640	82	(−)	0.1 g[b]
6	700	80	(−)	0.5 g[b]
7	760	75	(−)	1.3 g[b]

[a]: trace white solid.
[b]. biphenyl.

Table 6. Results of reactions using 5g of 500 mesh Al_2O_3 coating on 10g of pyrex glass wool as catalyst. Carrier gas: air (160 ml/min).

Run No.	Temp. (°C)	Recovery C_6H_6 (ml)	$FeCl_3$ Test	Products
1	400	90	(−)	
2	460	90	(−)	[a]
3	520	88	(−)	[a]
4	580	85	(−)	0.1 g[b]
5	640	82	(−)	0.3 g[b]
6	700	80	(−)	1.0 g[b]
7	760	75	(−)	3.4 g[b]
8	760	70	(−)	3.6 g[b]

[a]: trace white solid.
[b]: biphenyl.

Table 7. Results of reactions using 5g of silica gel coating on 10g of pyrex glass wool as catalyst. Carrier gas: N_2 (160 ml/min).

Run No.	Temp. (°C)	Recovery C_6H_6 (ml)	$FeCl_3$ Test	Products
1	400	90	(−)	
2	460	90	(−)	
3	520	87	(−)	[a]
4	580	85	(−)	[a]
5	640	80	(−)	0.1 g[b]
6	700	70	(−)	0.5 g[b] + C[c]
7	760	160	(−)	1.0 g[b] + C[c]

[a]: trace white solid.
[b]: biphenyl.
[c]: carbon.

Table 8. Results of reactions using 5g of silica gel coating on 10g of pyrex glass wool as catalyst. Carrier gas: air (160 ml/min).

Run No.	Temp. (°C)	Recovery C_6H_6 (ml)	$FeCl_3$ Test	Products
1	400	90	(−)	
2	460	90	(−)	
3	520	85	(−)	[a]
4	580	85	(−)	[a]
5	640	75	(−)	0.1 g[b]
6	700	60	(−)	0.5 g[b] + C[c]
7	700	60	(−)	0.5 g[b] + C[c]

[a]: trace white solid.
[b]: biphenyl.
[c]: carbon.

Table 9. Results of reactions using Ni-Al alloy powder (5g, containing 48% of Ni) coating on 10g of pyrex glass wool as catalyst. Carrier gas: N_2 (160 ml/min).

Run No.	Temp. (°C)	Recovery C_6H_6 (ml)	$FeCl_3$ Test	Products
1	400	90	(−)	
2	460	90	(−)	
3	520	86	(−)	[a]
4	580	84	(−)	[a]
5	640	82	(−)	0.1 g[b]
6	700	80	(−)	0.5 g[b]
7	760	76	(−)	1.2 g[b]
8	820	62	(−)	3.0 g[b] + C[c]

[a]: trace white solid.
[b]: biphenyl.
[c]: carbon.

Table 10. Results of reactions using Ni-Al alloy powder (5g, containing 48% of Ni) coating on 10g of pyrex glass wool as catalyst. Carrier gas: air (160 ml/min).

Run No.	Temp. (°C)	Recovery C_6H_6 (ml)	$FeCl_3$ Test	Products
1	400	90	(−)	
2	460	90	(−)	
3	520	88	(−)	[a]
4	580	84	(−)	0.1 g[b]
5	640	84	(−)	0.3 g[b]
6	700	80	(−)	1.0 g[b]
7	760	73	(−)	2.8 g[b]
8	820	65	(−)	3.5 g[b]

[a]: trace white solid.
[b]: biphenyl.

Table 11. Results of reactions using 5g of 25% Pt-quartz as catalyst. Carrier gas: N_2 (160 ml/min).

Run No.	Temp. (°C)	Recovery C_6H_6 (ml)	$FeCl_3$ Test	Products
1	400	90	(−)	
2	460	90	(−)	
3	520	90	(−)	[a]
4	580	85	(−)	0.1 g[b]
5	640	85	(−)	0.2 g[b]
6	700	80	(−)	0.5 g[b]
7	760	60	(−)	1.5 g[b] + C[c]

[a]: trace white solid.
[b]: biphenyl.
[c]: carbon.

Table 12. Results of reactions using 5g of 25% Pt-quartz as catalyst. Carrier gas: air (160 ml/min).

Run No.	Temp. (°C)	Recovery C_6H_6 (ml)	$FeCl_3$ Test	Products
1	400	90	(−)	
2	460	90	(−)	[a]
3	520	85	(−)	0.3 g[b]
4	580	85	(−)	0.5 g[b]
5	640	80	(−)	0.5 g[b] + C[c]
6	700	70	(−)	1.0 g[b] + C[c]
7	760	60	(−)	1.5 g[b] + C[c]

[a]: trace white solid.
[b]: biphenyl.
[c]: carbon.

Table 13. Results of reactions using 5g of V_2O_5 powder coating on 10g of pyrex glass wool as catalyst. Carrier gas: N_2 (160 ml/min).

Run No.	Temp. (°C)	Recovery C_6H_6 (ml)	$FeCl_3$ Test	Products
1	400	90	(−)	
2	460	90	(−)	
3	520	88	(−)	[a]
4	580	85	(−)	[a]
5	640	80	(−)	0.1 g[b]
6	700	75	(−)	0.5 g[b] + C[c]
7	760	70	(−)	1.2 g[b] + C[c]

[a]: trace solid.
[b]: biphenyl.
[c]: carbon.

Table 14. Results of reactions using 5g of V_2O_5 powder coating on 10g of pyrex glass wool as catalyst. Carrier gas: air (160 ml/min).

Run No.	Temp. (°C)	Recovery C_6H_6 (ml)	$FeCl_3$ Test	Products
1	400	90	(−)	
2	460	90	(−)	[a]
3	520	85	(−)	0.1 g[b]
4	580	80	(−)	1.0 g[b]
5	640	75	(−)	1.0 g[b] + C[c]
6	700	65	(−)	0.5 g[b] + C[c]
7	760	55	(−)	0.5 g[b] + C[c]
8[d]	580	75	(−)	1.0 g[b]
9[e]	580	75	(−)	1.5 g[b]
10[f]	580	80	(−)	1.0 g[b]

[a]: trace brown solid.
[b]: P-benzoquinone.
[c]: carbon.
[d]: $(C_6H_6) : (H_2O) = 1 : 3$
[e]: $(C_6H_6) : (H_2O) = 1 : 5$
[f]: $(C_6H_6) : (H_2O) = 1 : 0$

Table 15. Results of reaction using a copper pipe (7/8″ OD). Carrier gas: N_2 (160 ml/min).

Run No.	Temp. (°C)	Recovery C_6H_6 (ml)	$FeCl_3$ Test	Products
1	400	90	(−)	
2	460	90	(−)	
3	520	85	(−)	[a]
4	580	80	(−)	[a]
5	640	78	(−)	0.5 g[b]
6	700	70	(−)	0.5 g[b] + C[c]
7	760	60	(−)	1.0 g[b] + C[c]

[a]: trace solid.
[b]: biphenyl.
[c]: carbon.

Table 16. Results of reaction using a copper pipe (7/8″ OD). Carier gas: air (160 ml/min).

Run No.	Temp. (°C)	Recovery C_6H_6 (ml)	$FeCl_3$ Test	Products
1	400	90	(−)	
2	460	90	(+)	Trace brown liquid
3	520	80	(+)	0.1g brown liquid
4	580	75	(+)	0.5g brown liquid[c]
5	640	70	(+)	1.0g brown liquid[d]
6	700	65	(+)	1.0g brown liquid[e] +C
7[a]	640	70	(+)	1.0g brown liquid[c]
8[b]	640	68	(+)	1.0g brown liquid[d]

[a]: $(C_6H_6) : (H_2O) = 1 : 0$
[b]: $(C_6H_6) : (H_2O) = 1 : 3$
[c]: brown liquid with 50% phenol tested by G.C.
[d]: brown liquid with 70% phenol tested by G.C. (Chart 1).
[e]: 50% phenol tested by G.C.

Table 17. Results of reaction using 5g of V_2O_5/KH_2PO_2 mixture coating on 10g of pyrex glass wool as catalyst at the temperature of 580°C.
Carrier gas: air (160 ml/min).

Run No.	V_2O_5/KH_2PO_4 (g/g)	Recovery C_6H_6 (ml)	$FeCl_3$ Test	Products
1	4:1	80	(+)	0.8g P[a] trace br. liq.[b]
2	1:1	80	(+)	0.5g P[a] 0.2g br. liq.[c]
3	1:4	80	(+)	Trace brown gel[d]
4	0:1	80	(−)	Trace white solid

[a]: P-benzoquinone.
[b]: Contains 10% of phenol tested by G.C.
[c]: Contains 50% of phenol tested by G.C. (Chart 2).
[d]: Contains trace of phenol tested by G.C.

730, 700, and G.L.C. co-injection analysis is identical with the authentic sample. (Biphenyl from E. Merck Darmstadt). The yield of biphenyl increases with increasing temperature of the reactor. As the temperature is increased up to 820°C, carbon begins to deposit in the reactor. (Table 1).

In the presence of oxygen, at temperatures ranging from 400°–820°C biphenyl is again isolated as the sole product. (Table 2).

Next we successively introduced active carbon, aluminum oxide, silica gel, Ni-Al alloy powder, platinum and vanadium pentoxide into the reactor as catalysts, and replaced the stainless steel reactor pipe with a copper one to study the catalytic ability of copper.

In the presence of the catalysts, without oxygen, the only product again is biphenyl (Tables 3, 5, 7, 9, 11, 13 and 15). Using air as carrier gas and a temperature range of 400° to 820°C in the presence of active carbon, aluminum oxide, silica gel, Ni-Al alloy platinum the only product is biphenyl also. (Tables 4, 6, 8, 10 and 12). The catalysts can not facilitate reaction (1) and except for vanadium pentoxide and copper, they can also not facilitate reaction (2).

We suggest that at high temperatures benzene homolyzes to form phenyl radicals and then undergoes coupling to form biphenyl.

$$C_6H_6 \longrightarrow C_6H_5\cdot + H\cdot \quad (3)$$

$$2C_6H_5\cdot \longrightarrow C_6H_5-C_6H_5 \quad (4)$$

If phenyl radicals are present the following reaction steps may produce phenol:

$$H_2O \longrightarrow HO\cdot + H\cdot \quad (5)$$

$$C_6H_5\cdot + HO\cdot \longrightarrow C_6H_5OH \quad (6)$$

or

$$C_6H_5\cdot + H_2O \longrightarrow C_6H_5OH + H\cdot \quad (7)$$

From table 1, we understand that reactions (6) and (7) do not occur, and suggest that after formation of the phenyl radical three possible reactions may follow:

(a) Recombination with H· to form benzene.
(b) Following reaction (4) coupling occurs to form biphenyl.
(c) Reaction with water to form phenol through reactions (6) or (7).

The thermal stability of water is very high. At 1027°C only 0.00266% decomposes[7], and at a temperature range of 400° to 820° reaction (5) can not occur to any extent. From the heat of reaction (3), (4) and (7) (ΔH = 103 Kcal/mole, −100 Kcal/mole and 16 Kcal/mole respectively)[8], we can easily understand that reaction (4) and the reverse of reaction (3) is more favored. If there is a HO· free radical present, reaction (6) (ΔH = −110 Kcal/mole)[8] may be favored, too. But the catalysts chosen fail to facilitate the reaction (5).

In the presence of oxygen the yield of biphenyl increases. The coupling of phenyl radicals is increased which shows that oxygen reacts with H· from reaction (3) and increases the life time or concentration of the phenyl radical. From the fact that in Tables 2, 4, 6, 8, 10 and 12 no phenol is produced, we understand that increasing the life time or concentration of the phenyl radical does not make it react with water to form phenol.

Over vanadium pentoxide and in the presence of oxygen we can get a yellow solid identified to be *p*-benzoquinone (IR spectrum

ν max cm^{-1}: 3080, 1080, 1600, 1318, 1090, 1075, 945, 900, 742 and GLC co-injection analysis are identical with that of the authentic sample. *p*-benzoquinone from E. Merk Darmstadt), with the best yield at 580°C. The ferric chloride test shows no phenol present in water and G.L.C. shows no phenol in the organic layer either. However there is some biphenyl present (Table 14). Formation of *p*-benzoquinone may occur by the following route:

(i) Vanadium pentoxide catalizes the reaction of the phenyl radical oxidation directly into *p*-benzoquinone

$$C_6H_5\cdot \xrightarrow[-H]{V_2O_5,\ O_2} O=\langle\rangle=O \qquad (8)$$

(ii) The phenyl radical reacts with vanadium pentoxide to form phenol or its derivatives and further oxidizes to form *p*-benzoquinone before escaping from the surface of vanadium pentoxide.

$$C_6H_5\cdot \xrightarrow{V_2O_5} [C_6H_5OH] \xrightarrow[O_2]{V_2O_5} O=\langle\rangle=O \qquad (9)$$

In order to understand the reaction through (i) and (ii), we tried to increase the surface acidity of V_2O_5 and to decrease its affinity to phenol by mixing vanadium pentoxide with KH_2PO_4. The products show that some phenol is produced, and we can be sure that benzene in the presence of vanadium pentoxide oxidizes to phenol or its derivatives and then further oxidizes to *p*-benzoquinone. (Table 17).

In the copper pipe with air as carrier gas, having a reactor temperature of 460°C, the ferric chloride test begins to show that phenol produced (IR spectrum ν max cm^{-1}: 3200 (broad), 1605, 1520, 1485, 1240, 1080, 890, 830, 760, 700 and G.L.C. analysis identical with authentic sample; phenol 98% GR from E. Merk Darmstadt) gives the best yield at 640°C (Table 16). G.L.C. shows that in addition to phenol as the product, it contains little biphenyl and *p*-benzoquinone. (Chart 1).

Comparing the G.L.C. analysis of products of Table (16) and Table (17), (Chart 1 and Chart 2), we find that both of them seem

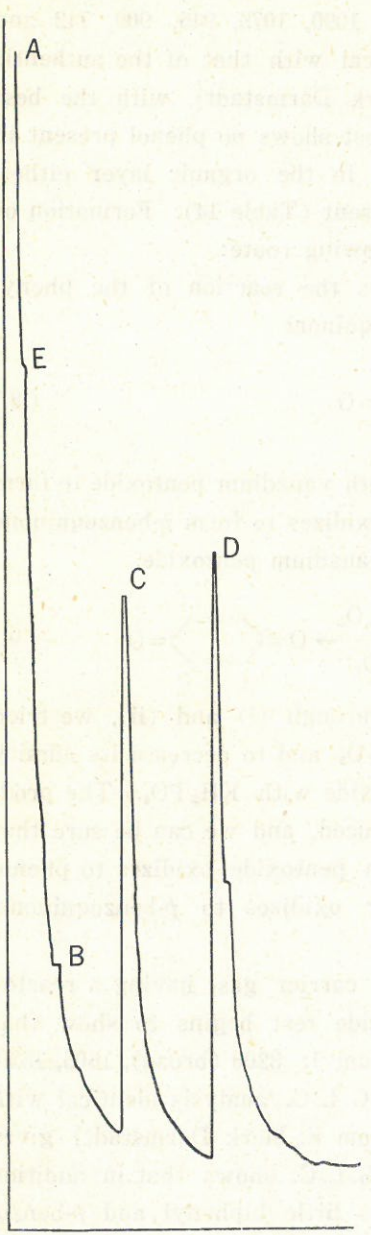

Chart 1: G. L. C. analysis of products of run No. 5, Table 16

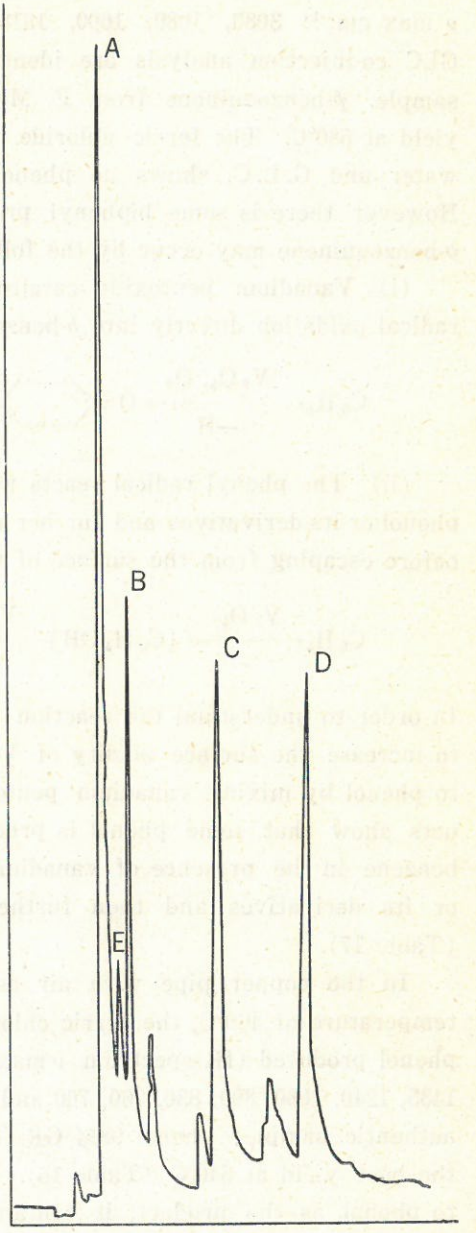

Chart 2: G. L. C. analysis of products of run No. 2, Table 17

to have the same components, such as phenol (peak A), *p*-benzoquinone (peak B) biphenyl (peak C) and two unidentified components (peaks D and E). Therefore we suggest that the formation of phenol over copper and over vanadium pentoxide may have a similar mechanism (intermediate).

We suggest that the formation of phenol and *p*-benzoquinone over vanadium pentoxide occurs according to the following steps:

$$C_6H_5\cdot + V_2O_5 \longrightarrow (C_6H_5{}^*\text{-O-}V_2O_4) \xrightarrow[\text{or } H\cdot]{H^{\oplus}} C_6H_5OH + 2\,VO_2 \qquad (10)$$

$$C_6H_5OH + V_2O_5 \longrightarrow O=\langle\bigcirc\rangle=O + V_2O_3 + H_2O \qquad (11)$$

$$V_2O_3 + 2\,VO_2 + O_2 \xrightarrow{\Delta} V_2O_5 \qquad (12)$$

The phenyl radical reacts with V_2O_5 to form a phO-V bond and then changes into phenol, most of which further oxidizes to *p*-benzoquinone. The lower oxidation state of vanadium is regenerated as vanadium pentoxide by reaction with oxygen, and we suggest that on the surface of the copper pipe there is a thin film of cupric oxide which reacts with the phenyl radical to form cuprous phenoxide and then is reduced to phenol and copper.

$$C_6H_5\cdot + CuO \longrightarrow (C_6H_5O\text{-}Cu) \xrightarrow{H\cdot} C_6H_5OH + Cu \qquad (13)$$

$$C_6H_5OH + CuO \longrightarrow O=\langle\bigcirc\rangle=O + Cu \qquad (14)$$

$$Cu + O_2 \xrightarrow{\Delta} CuO \qquad (16)$$

In both cases we find that a phenyl radical can react both with vanadium pentoxide and cupric oxide to form a phO-metal intermediate which reacts with the same reactive species and that it would produce the same products shown in charts 1 and 2, for components of peaks D and E.

Further studies will be made to increase the yield of phenol

and *p*-benzoquinone, to identify the components of peaks D and E (Charts 1 and 2) and to understand the mechanism of phenol formation.

REFERENCES

(1) Shreve, R.N., "*Chemical Process Industries*" 3rd edition p. 676. McGraw-Hill Inc. (1967).
(2) C.A. 13586 f **65**, (1966).
(3) C.A. 42053 c **74**, (1971).
(4) C.A. 113522 e **77**, (1972).
(5) C.A. 614275 **77**, (1972).
(6) C.A. 126006 f **80**, (1974).
(7) Bailar Jr. J, C., *et al. University Chemistry* p. 47 (1965).
(8) Benson, S.W., *J. Chem. Educ.* **42**, 502 (1965).

CONTRIBUTORS TO THIS NUMBER

Yi-Ching Yen 顏一清 is professor of mathematics at Fu Jen University.

Nei-Mao Chen 陳迺懋 is associate professor of mathematics at Fu Jen University.

Jen-I Chen 陳振益 is professor of physics at Fu Jen University.

Zuon-Hua Luo 羅榮華 is professor of electronic engineering at Fu Jen University.

Frank E. Budenholzer, SVD 柏殿宏 is associate professor of chemistry at Fu Jen University.

Yung-Nan Chen 陳榮男 is associate professor of chemistry at Fu Jen University.

PRINTED BY

Ching Hua Press Co., LTD., Taipei